DESY–13–245
December 2013

Measurement of neutral current $e^{\pm}p$ cross sections at high Bjorken x with the ZEUS detector

ZEUS Collaboration

Abstract

The neutral current $e^{\pm}p$ cross section has been measured up to values of Bjorken $x \cong 1$ with the ZEUS detector at HERA using an integrated luminosity of $187\,\mathrm{pb}^{-1}$ of $e^{-}p$ and $142\,\mathrm{pb}^{-1}$ of $e^{+}p$ collisions at $\sqrt{s} = 318\,\mathrm{GeV}$. Differential cross sections in x and Q^2, the exchanged boson virtuality, are presented for $Q^2 \geq 725\,\mathrm{GeV}^2$. An improved reconstruction method and greatly increased amount of data allows a finer binning in the high-x region of the neutral current cross section and leads to a measurement with much improved precision compared to a similar earlier analysis. The measurements are compared to Standard Model expectations based on a variety of recent parton distribution functions.

The ZEUS Collaboration

H. Abramowicz[27,t], I. Abt[21], L. Adamczyk[8], M. Adamus[34], R. Aggarwal[4,a], S. Antonelli[2], O. Arslan[3], V. Aushev[16,17,n], Y. Aushev,[17,n,o], O. Bachynska[10], A.N. Barakbaev[15], N. Bartosik[10], O. Behnke[10], J. Behr[10], U. Behrens[10], A. Bertolin[23], S. Bhadra[36], I. Bloch[11], V. Bokhonov[16,n], E.G. Boos[15], K. Borras[10], I. Brock[3], R. Brugnera[24], A. Bruni[1], B. Brzozowska[33], P.J. Bussey[12], A. Caldwell[21], M. Capua[5], C.D. Catterall[36], J. Chwastowski[7,d], J. Ciborowski[33,w], A.M. Cooper-Sarkar[22], M. Corradi[1], F. Corriveau[18], G. D'Agostini[26], R.K. Dementiev[20], R.C.E. Devenish[22], G. Dolinska[10], V. Drugakov[11], S. Dusini[23], J. Ferrando[12], J. Figiel[7], B. Foster[13,k], G. Gach[8], A. Garfagnini[24], A. Geiser[10], A. Gizhko[10], L.K. Gladilin[20], O. Gogota[17], Yu.A. Golubkov[20], J. Grebenyuk[10], I. Gregor[10], G. Grzelak[33], O. Gueta[27], M. Guzik[8], W. Hain[10], G. Hartner[36], D. Hochman[35], R. Hori[14], Z.A. Ibrahim[6], Y. Iga[25], M. Ishitsuka[28], A. Iudin[17,o], F. Januschek[10], I. Kadenko[17], S. Kananov[27], T. Kanno[28], U. Karshon[35], M. Kaur[4], P. Kaur[4,a], L.A. Khein[20], D. Kisielewska[8], R. Klanner[13], U. Klein[10,f], N. Kondrashova[17,p], O. Kononenko[17], Ie. Korol[10], I.A. Korzhavina[20], A. Kotański[9], U. Kötz[10], N. Kovalchuk[17,q], H. Kowalski[10], O. Kuprash[10], M. Kuze[28], B.B. Levchenko[20], A. Levy[27], V. Libov[10], S. Limentani[24], M. Lisovyi[10], E. Lobodzinska[10], W. Lohmann[11], B. Löhr[10], E. Lohrmann[13], A. Longhin[23,s], D. Lontkovskyi[10], O.Yu. Lukina[20], J. Maeda[28,u], I. Makarenko[10], J. Malka[10], J.F. Martin[31], S. Mergelmeyer[3], F. Mohamad Idris[6,c], K. Mujkic[10,g], V. Myronenko[10,h], K. Nagano[14], A. Nigro[26], T. Nobe[28], D. Notz[10], R.J. Nowak[33], K. Olkiewicz[7], Yu. Onishchuk[17], E. Paul[3], W. Perlański[33,x], H. Perrey[10], N.S. Pokrovskiy[15], A.S. Proskuryakov[20], M. Przybycień[8], A. Raval[10], P. Roloff[10,i], I. Rubinsky[10], M. Ruspa[30], V. Samojlov[15], D.H. Saxon[12], M. Schioppa[5], W.B. Schmidke[21,r], U. Schneekloth[10], T. Schörner-Sadenius[10], J. Schwartz[18], L.M. Shcheglova[20], R. Shevchenko[17,o], O. Shkola[17,q], I. Singh[4,b], I.O. Skillicorn[12], W. Słomiński[9,e], V. Sola[13], A. Solano[29], A. Spiridonov[10,j], L. Stanco[23], N. Stefaniuk[10], A. Stern[27], T.P. Stewart[31], P. Stopa[7], J. Sztuk-Dambietz[13], D. Szuba[13], J. Szuba[10], E. Tassi[5], T. Temiraliev[15], K. Tokushuku[14,l], J. Tomaszewska[33,y], A. Trofymov[17,q], V. Trusov[17], T. Tsurugai[19], M. Turcato[13], O. Turkot[10,h], T. Tymieniecka[34], A. Verbytskyi[21], O. Viazlo[17], R. Walczak[22], W.A.T. Wan Abdullah[6], K. Wichmann[10,h], M. Wing[32,v], G. Wolf[10], S. Yamada[14], Y. Yamazaki[14,m], N. Zakharchuk[17,q], A.F. Żarnecki[33], L. Zawiejski[7], O. Zenaiev[10], B.O. Zhautykov[15], N. Zhmak[16,n], D.S. Zotkin[20]

[1] *INFN Bologna, Bologna, Italy* [A]
[2] *University and INFN Bologna, Bologna, Italy* [A]
[3] *Physikalisches Institut der Universität Bonn, Bonn, Germany* [B]
[4] *Panjab University, Department of Physics, Chandigarh, India*
[5] *Calabria University, Physics Department and INFN, Cosenza, Italy* [A]
[6] *National Centre for Particle Physics, Universiti Malaya, 50603 Kuala Lumpur, Malaysia* [C]
[7] *The Henryk Niewodniczanski Institute of Nuclear Physics, Polish Academy of Sciences, Krakow, Poland* [D]
[8] *AGH-University of Science and Technology, Faculty of Physics and Applied Computer Science, Krakow, Poland* [D]
[9] *Department of Physics, Jagellonian University, Cracow, Poland*
[10] *Deutsches Elektronen-Synchrotron DESY, Hamburg, Germany*
[11] *Deutsches Elektronen-Synchrotron DESY, Zeuthen, Germany*
[12] *School of Physics and Astronomy, University of Glasgow, Glasgow, United Kingdom* [E]
[13] *Hamburg University, Institute of Experimental Physics, Hamburg, Germany* [F]
[14] *Institute of Particle and Nuclear Studies, KEK, Tsukuba, Japan* [G]
[15] *Institute of Physics and Technology of Ministry of Education and Science of Kazakhstan, Almaty, Kazakhstan*
[16] *Institute for Nuclear Research, National Academy of Sciences, Kyiv, Ukraine*
[17] *Department of Nuclear Physics, National Taras Shevchenko University of Kyiv, Kyiv, Ukraine*
[18] *Department of Physics, McGill University, Montréal, Québec, Canada H3A 2T8* [H]
[19] *Meiji Gakuin University, Faculty of General Education, Yokohama, Japan* [G]
[20] *Lomonosov Moscow State University, Skobeltsyn Institute of Nuclear Physics, Moscow, Russia* [I]
[21] *Max-Planck-Institut für Physik, München, Germany*
[22] *Department of Physics, University of Oxford, Oxford, United Kingdom* [E]
[23] *INFN Padova, Padova, Italy* [A]
[24] *Dipartimento di Fisica dell' Università and INFN, Padova, Italy* [A]
[25] *Polytechnic University, Tokyo, Japan* [G]
[26] *Dipartimento di Fisica, Università 'La Sapienza' and INFN, Rome, Italy* [A]
[27] *Raymond and Beverly Sackler Faculty of Exact Sciences, School of Physics, Tel Aviv University, Tel Aviv, Israel* [J]
[28] *Department of Physics, Tokyo Institute of Technology, Tokyo, Japan* [G]
[29] *Università di Torino and INFN, Torino, Italy* [A]
[30] *Università del Piemonte Orientale, Novara, and INFN, Torino, Italy* [A]
[31] *Department of Physics, University of Toronto, Toronto, Ontario, Canada M5S 1A7* [H]
[32] *Physics and Astronomy Department, University College London, London, United Kingdom* [E]
[33] *Faculty of Physics, University of Warsaw, Warsaw, Poland*

[34] *National Centre for Nuclear Research, Warsaw, Poland*
[35] *Department of Particle Physics and Astrophysics, Weizmann Institute, Rehovot, Israel*
[36] *Department of Physics, York University, Ontario, Canada M3J 1P3* [H]

[A] supported by the Italian National Institute for Nuclear Physics (INFN)
[B] supported by the German Federal Ministry for Education and Research (BMBF), under contract No. 05 H09PDF
[C] supported by HIR grant UM.C/625/1/HIR/149 and UMRG grants RU006-2013, RP012A-13AFR and RP012B-13AFR from Universiti Malaya, and ERGS grant ER004-2012A from the Ministry of Education, Malaysia
[D] supported by the National Science Centre under contract No. DEC-2012/06/M/ST2/00428
[E] supported by the Science and Technology Facilities Council, UK
[F] supported by the German Federal Ministry for Education and Research (BMBF), under contract No. 05h09GUF, and the SFB 676 of the Deutsche Forschungsgemeinschaft (DFG)
[G] supported by the Japanese Ministry of Education, Culture, Sports, Science and Technology (MEXT) and its grants for Scientific Research
[H] supported by the Natural Sciences and Engineering Research Council of Canada (NSERC)
[I] supported by RF Presidential grant N 3920.2012.2 for the Leading Scientific Schools and by the Russian Ministry of Education and Science through its grant for Scientific Research on High Energy Physics
[J] supported by the Israel Science Foundation

[a] also funded by Max Planck Institute for Physics, Munich, Germany
[b] also funded by Max Planck Institute for Physics, Munich, Germany, now at Sri Guru Granth Sahib World University, Fatehgarh Sahib
[c] also at Agensi Nuklear Malaysia, 43000 Kajang, Bangi, Malaysia
[d] also at Cracow University of Technology, Faculty of Physics, Mathematics and Applied Computer Science, Poland
[e] partially supported by the Polish National Science Centre projects DEC-2011/01/B/ST2/03643 and DEC-2011/03/B/ST2/00220
[f] now at University of Liverpool, United Kingdom
[g] also affiliated with University College London, UK
[h] supported by the Alexander von Humboldt Foundation
[i] now at CERN, Geneva, Switzerland
[j] also at Institute of Theoretical and Experimental Physics, Moscow, Russia
[k] Alexander von Humboldt Professor; also at DESY and University of Oxford
[l] also at University of Tokyo, Japan
[m] now at Kobe University, Japan
[n] supported by DESY, Germany
[o] member of National Technical University of Ukraine, Kyiv Polytechnic Institute, Kyiv, Ukraine
[p] now at DESY ATLAS group
[q] member of National University of Kyiv - Mohyla Academy, Kyiv, Ukraine
[r] now at BNL, USA
[s] now at LNF, Frascati, Italy
[t] also at Max Planck Institute for Physics, Munich, Germany, External Scientific Member
[u] now at Tokyo Metropolitan University, Japan
[v] also supported by DESY
[w] also at Łódź University, Poland
[x] member of Łódź University, Poland
[y] now at Polish Air Force Academy in Deblin

1 Introduction

Measurements of deep inelastic scattering (DIS) cross sections in lepton-proton collisions constitute an essential ingredient in probing the structure of the proton, which is represented by the parton distribution functions (PDFs). At large Bjorken x, uncertainties in the PDFs are often dominant uncertainty in the prediction of the cross section in perturbative QCD (pQCD).

The data span Bjorken x values in the range $6 \cdot 10^{-7} - 0.65$ and of intermediate-boson virtuality, Q^2, in the range $0.045 - 40\,000\,\mathrm{GeV}^2$ [1]. In the region of applicability of pQCD, the DIS cross-section measurements in $e^{\pm}p$ at HERA are precise enough to allow PDFs to be extracted solely from these data [1].

Most of the data available for $x \geq 0.7$ [2,3] have been obtained in fixed-target experiments in a Q^2 range where pQCD may not be fully applicable. In order to extend PDFs to $x = 1$, a parametrisation of the form $(1-x)^{\beta}$ is assumed. Such a behaviour is expected from counting rules [4] with the power β further constrained by the momentum-sum rule. The HERA storage ring, where 920 GeV protons collided with 27.5 GeV electrons or positrons, offered an opportunity to probe the large-x region, up to the kinematic limit, at high Q^2 where pQCD and DGLAP evolution dynamics are applicable.

The ZEUS collaboration published first results on the high-x behaviour of the cross section for $Q^2 > 600$ GeV^2 [5] using data taken in 1996 – 2000. The neutral current (NC) cross-section measurements presented in this paper are based on data collected in 2004 – 2007, with integrated luminosities of $187\,\mathrm{pb}^{-1}$ for e^-p and $142\,\mathrm{pb}^{-1}$ for e^+p scattering, i.e. a factor ten and two, respectively, larger than in the previous high-x ZEUS studies [5]. Given the much larger data sample and an improved analysis procedure, the uncertainties are substantially reduced. The data sets used for this analysis overlap with previously published ZEUS results [6, 7]. The finer binning in the medium- and large-x regions, as well as the extension of the cross-section measurements to $x \cong 1$, are expected to provide constraints on the PDFs at high x, where the contribution of valence quarks is important.

2 Kinematic variables and cross sections

Inclusive deep inelastic lepton-proton scattering can be described in terms of the kinematic variables x, y and Q^2. The variable Q^2 is defined as $Q^2 = -q^2 = -(k - k')^2$, where k and k' are the four-momenta of the incoming and scattered lepton, respectively. Bjorken x is defined as $x = Q^2/2P \cdot q$, where P is the four-momentum of the incoming proton. The fraction of the lepton energy transferred to the proton in its rest frame is given by

$y = P \cdot q / P \cdot k$. The variables x, y and Q^2 are related by $Q^2 = sxy$, where s, the centre-of-mass-energy squared, is given by $s = 4E_eE_p$, and E_e and E_p are the initial energies of the electron and proton, respectively.

The electroweak Born-level cross section for the $e^{\pm}p$ NC interaction is given by [8, 9]

$$\frac{d^2\sigma(e^{\pm}p)}{dxdQ^2} = \frac{2\pi\alpha^2}{xQ^4}[Y_+\tilde{F}_2(x,Q^2) \mp Y_-x\tilde{F}_3(x,Q^2) - y^2\tilde{F}_L(x,Q^2)], \quad (1)$$

where α is the fine-structure constant, $Y_{\pm} = 1 \pm (1-y)^2$, and $\tilde{F}_2(x,Q^2)$, $\tilde{F}_3(x,Q^2)$ and $\tilde{F}_L(x,Q^2)$ are generalised structure functions. Next-to-leading-order (NLO) QCD calculations predict that the contribution of the longitudinal structure function, $\tilde{F}_L$, to $d^2\sigma/dxdQ^2$ is approximately 1.5%, averaged over the kinematic range considered.

Photon exchange dominates the cross section at low Q^2 and is described by $\tilde{F}_2$ and $\tilde{F}_L$. It is only at Q^2 values comparable to M_Z^2 that the γ/Z interference and the Z exchange terms become important and the $\tilde{F}_3$ term contributes significantly to the cross section. The sign of the $\tilde{F}_3$ term in Eq. (1) shows that electroweak effects increase (decrease) the e^-p (e^+p) cross sections.

Reduced cross sections, $\tilde{\sigma}$, for e^-p and e^+p scattering are defined as

$$\tilde{\sigma}^{e^{\pm}p} = \frac{xQ^4}{2\pi\alpha^2}\frac{1}{Y_+}\frac{d^2\sigma(e^{\pm}p)}{dxdQ^2}. \quad (2)$$

The generalised structure functions depend linearly on the longitudinal polarisation of the electron[1] beam. The extracted cross sections correspond to unpolarised lepton beams.

3 Experimental set-up

A detailed description of the ZEUS detector can be found elsewhere [10]. A brief outline of the components that are most relevant for this analysis is given below.

In the kinematic range of the analysis, charged particles were tracked in the central tracking detector (CTD) [11], the microvertex detector (MVD) [12] and the straw-tube tracker (STT) [13]. The CTD and the MVD operated in a magnetic field of 1.43 T provided by a thin superconducting solenoid. The CTD drift chamber covered the polar-angle[2] region $15^\circ < \theta < 164^\circ$. The MVD silicon tracker consisted of a barrel (BMVD) and

[1] Here and in the following the term electron denotes generically both the electron and the positron.

[2] The ZEUS coordinate system is a right-handed Cartesian system, with the Z axis pointing in the proton beam direction, referred to as the "forward direction", and the X axis pointing towards the centre of HERA. The coordinate origin is at the nominal interaction point.

a forward (FMVD) section. The BMVD provided polar-angle coverage for tracks with three measurements from 30° to 150°. The FMVD extended the polar-angle coverage in the forward region to 7°. The STT covered the polar-angle region $5° < \theta < 25°$. For CTD-MVD tracks that pass through all nine CTD superlayers, the momentum resolution was $\sigma(p_T)/p_T = 0.0029 p_T \oplus 0.0081 \oplus 0.0012/p_T$, with p_T in GeV.

The high-resolution uranium–scintillator calorimeter (CAL) [14] consisted of three parts: the forward (FCAL), the barrel (BCAL) and the rear (RCAL) calorimeters. Each part was subdivided transversely into towers and longitudinally into one electromagnetic section (EMC) and either one (in RCAL) or two (in BCAL and FCAL) hadronic sections (HAC). The smallest subdivision of the calorimeter was called a cell. The CAL energy resolutions, as measured under test-beam conditions, were $\sigma(E)/E = 0.18/\sqrt{E}$ for electrons and $\sigma(E)/E = 0.35/\sqrt{E}$ for hadrons, with E in GeV.

The luminosity was measured using the Bethe–Heitler reaction $ep \to e\gamma p$ by a luminosity detector which consisted of independent lead–scintillator calorimeter [15] and magnetic spectrometer [16] systems. The systematic uncertainty on the measured luminosity was 1.8%.

The analysed data were collected with longitudinally polarised e^- and e^+ beams. The beam polarisation was measured using two independent polarimeters, a transverse [17,18] and a longitudinal polarimeter [19]. The luminosity-weighted polarisations for the e^- beam were $+0.28$ and -0.28 and for the e^+ beam $+0.33$ and -0.36. Since the level of polarisation is very similar for the right-handed and left-handed lepton beams, the correction applied to obtain the unpolarised cross sections was very small.

4 Monte Carlo samples

Monte Carlo (MC) simulations were used to determine the efficiency for selecting the events, the accuracy of kinematic reconstruction, to estimate the background rates and to extract the cross section in the kinematic region of interest. A sufficient number of events were generated to ensure negligible statistical uncertainties compared to data.

Neutral current DIS events were simulated including leading-order electroweak radiative effects, using the Heracles [20] program with the Djangoh 1.6 [21] interface to the fragmentation and hadronisation programs and using HERAPDF1.5 PDFs [22]. To study the effect of the modelling of QCD radiation on the final results, two independent NC samples were generated, one with the Meps model of Lepto 6.5.1 [23] and the other with the colour-dipole model of Ariadne 4.12 [24]. Both programs use the Lund string model as implemented in Jetset [25] for hadronisation. A linear combination of the two MC samples was found to give the best description of the jet variables as discussed in

Section 7.1. This combination was then used to extract the central values of the reduced cross sections.

Hard photoproduction, a potential source of background, was simulated using HERWIG 5.9 [26]. QED Compton events, another potential source of background, were generated using the GRAPE MC generator [27].

The ZEUS detector response was simulated using a program based on GEANT 3.21 [28]. The generated events were passed through the detector simulation, subjected to the same trigger requirements as the data and processed by the same reconstruction programs.

5 Event reconstruction

A typical NC high-Q^2 and high-x event consists of the scattered electron and a high-energy collimated jet of particles in the direction of the struck quark. The electron and the jet are balanced in transverse momentum. The proton remnant mostly disappears down the beam pipe. The x and Q^2 of events, in which the jet is well contained in the detector, may be determined by various techniques, such as the double-angle (DA) method [29, 30]. However, the maximum x value that can be reached is limited by the fact that at the low values of y typical of these events, the uncertainty on $x = Q^2/ys$ increases as $\Delta x/x \sim 1/y^2$.

An improved x reconstruction is achieved by observing that, in the limit of $x \to 1$, the energy of the struck quark represented by the collimated jet is $E_{\rm jet} \cong xE_p$. The exact expression for x is

$$x = \frac{E_{\rm jet}(1+\cos\theta_{\rm jet})}{2E_p\left(1-\frac{E_{\rm jet}(1-\cos\theta_{\rm jet})}{2E_e}\right)}\,, \tag{3}$$

where $\theta_{\rm jet}$ is the scattering angle of the jet.

As x increases and the jet associated with the struck quark disappears down the beam-pipe, the ability to reconstruct x is limited by the energy loss. However, in these events, the cross section integrated from a certain limit in x, $x_{\rm edge}$, up to $x = 1$ can be extracted. The value of $x_{\rm edge}$ below which the jet is fully contained in the detector depends on Q^2 and the higher the Q^2, the higher the value of $x_{\rm edge}$. The above observation constitutes the essence of the methodology applied in an earlier ZEUS publication [5].

In the analysis presented here, two improvements were introduced. Since, in these events, the scattered electron is very well measured in the detector, for the one-jet events, which statistically dominate the high-Q^2 and high-x NC samples, the measured value of $E_{\rm jet}$ in Eq. (3) is replaced by

$$E_{\rm jet} = E_T^e/\sin\theta_{\rm jet}\,, \tag{4}$$

as the transverse energy of the (massless) jet is balanced by the transverse energy of the scattered electron, E_T^e, and the uncertainty on the electron-energy scale and resolution is smaller than that for the hadronic component. Hard QCD processes present in DIS, such as boson-gluon fusion or QCD Compton, may lead to extra jets in the events. The analysis is thus extended to include multi-jet events. For the latter, the smallest bias on the x reconstruction was found for a modified Jacquet-Blondel method [31], in which

$$x = \frac{(E_T^{\rm jets})^2}{s(1-y_{\rm jets})y_{\rm jets}}\,, \tag{5}$$

where $E_T^{\rm jets}$ is the vector sum over the transverse-energy vectors of individual jets and $y_{\rm jets} = \sum_{\rm jets} E_i(1-\cos\theta_i)/2E_e$, where E_i and θ_i denote the energy and scattering angle of jet i and the sum runs over all jets. This approach is less sensitive to the contribution of particles that are not assigned to any jets.

The value of Q^2 is calculated from the measured scattered-electron energy, $E_e^{'}$, and scattering angle, θ_e, as

$$Q^2 = 2E_eE_e^{'}(1+\cos\theta_e)\,. \tag{6}$$

This provides the best resolution for non-radiative events.

5.1 Electron reconstruction

Calorimeter and CTD information [30] is used to identify the scattered electron and to determine its energy and scattering angle. The electron candidate is required to be isolated and matched to a well measured track if it lies in the CTD acceptance range ($20^\circ < \theta_e < 150^\circ$). The energy of the electron is taken from the calorimeter information. The scattering angle is determined either from the track measurement, for candidates within the CTD acceptance, or from the position reconstructed in the CAL and the interaction vertex.

If the electron candidate is found in the BCAL, the measured energy is corrected for non-uniformities in the response near the module and cell edges and for shower sampling variations. The absolute energy scale is determined using events from the kinematic peak, i.e. low-y events for which the expected electron energy, $E_{\rm KP}$, can be inferred from the scattering angle. The linearity of the energy response is then checked by comparing $E_e^{'}$ with the energy predicted by the DA approach. The same procedure was applied on data and MC. The comparison of the distributions $E_e^{'}/E_{\rm KP}$ in the data and in the MC is shown in Fig. 1 (a) and (b) for $y < 0.1$. Very good agreement is observed. The most probable values, obtained from Gaussian fits around the peak to data and MC, agree within 0.5%, which is taken as an estimate of the systematic uncertainty on the electron scale.

The electron energy resolution in the MC was found to be 5% for $E_e^{'} > 15$ GeV, and improves to 3% for electron energies above 50 GeV. The widths of the $E_e^{'}/E_{\rm KP}$ distributions in data and in MC agree within 10%, which is taken as an estimate of the systematic uncertainty on the energy resolution.

The angular resolution is about 0.6 mrad in the forward region and increases to 0.7 mrad in the central region. The Q^2 resolution is fairly constant throughout the range of the analysis and is dominated by the electron-energy resolution.

The systematic uncertainties of the absolute energy scale, the energy resolution and the scattering angle were validated by a procedure based on the kinematic fit to the reconstructed NC events, for which the fit is over-constrained (see Section 5.3).

The track-matching efficiency was found to be slightly lower in the data than in the MC and was corrected for. For the kinematic range studied here and after applying the selection cuts described in Section 6, the electron-detection efficiency is close to 100%.

5.2 Jet reconstruction

The jets were reconstructed in the laboratory frame using the inclusive k_T algorithm with the radius parameter R set to 1 in the massless scheme [32]. The algorithm was applied to the hadronic final state reconstructed using a combination of track and CAL information, excluding the cells and the track associated with the scattered electron. The selected tracks and CAL clusters were treated as massless energy-flow objects (EFOs) [33]. The jet variables are defined according to the Snowmass convention [34],

$$E_T^{\rm jet} = \sum_i E_{T,i} \ , \quad \eta_{\rm jet} = \frac{\sum_i E_{T,i}\eta_i}{E_T^{\rm jet}},$$
$$\theta_{\rm jet} = 2\tan^{-1}(e^{-\eta_{\rm jet}}) \ , \quad E_{\rm jet} = \sum_i E_i,$$

where E_i, $E_{T,i}$ and η_i are the energy, transverse energy and pseudorapidity of the EFOs, respectively. A jet is required to have a minimum transverse energy of 10 GeV. Events for which no jet was found are called zero-jet events.

The calibration of the jet-energy scale was performed through the transverse-momentum balance between the electron and the jet. Only one-jet events were selected for this procedure. A comparison between data and MC is shown in Fig. 1 (c)–(f), separately for jets found in the BCAL and in the FCAL. Very good agreement is found. This calibration procedure is estimated to yield a 1% uncertainty on the jet-energy scale and a 5% uncertainty on the jet-energy resolution.

For one-jet events, the expected angle of the jet, $\gamma_{\rm jet}$, may be inferred from the scattered-electron energy and angle. A comparison between the distributions of the ratio $\gamma_{\rm jet}/\theta_{\rm jet}$ in data and in MC demonstrated a good agreement both in the most probable values (to better than 0.5%) and in the widths (to better than 10%). In the estimate of systematic uncertainties, the variation in $\theta_{\rm jet}$ is replaced by a possible misalignment between data and MC of 5 mm in the position of the jet on the face of the calorimeter.

As in the case of electron reconstruction, the final values for the jet-energy scale, the jet-energy resolution, their uncertainties, as well as the uncertainties on the scattering angle of the jets were validated by the kinematic-fit procedure.

The jet angular resolution and to a smaller degree its energy resolution were propagated to the resolution on the reconstructed x value. For one-jet events, which constitute about 90% of the sample, the x resolution is about 0.01 at $x \simeq 0.15$, increases to 0.03 at $x = 0.35$ and remains constant at this value up to $x_{\rm edge}$. The x resolution for multi-jet events is about a factor of two worse.

5.3 Kinematic fit

The information on the kinematics of each NC event is over-constrained by the fact that both the electron variables and the hadronic variables are available. An event-by-event kinematic fit using the BAT package [35] was performed on the data and MC samples to study the description of the one-jet data by the MC simulation [36]. The inputs to the fit were the measured energy and angle of the electron and the energy and angle of the jet.

The output of the fit was the kinematic variables x, y and the energy of a possible intial-state radiative (ISR) photon. Bayesian inference was used,

$$P(x, y, E_\gamma|\vec{D}) \propto P(\vec{D}|x, y, E_\gamma) P_0(x, y, E_\gamma)\,,$$

where E_γ represents the energy of the ISR photon and $\vec{D}$ is the set of measured quantities. Simple priors were chosen to reflect the basic features of the DIS cross-section dependence on (x, y) and of the bremsstrahlung cross section on E_γ,

$$\begin{aligned} P_0(x, y, E_\gamma) &= P_0(x, y) P_0(E_\gamma) \\ P_0(x, y) &\propto \frac{(1-x)^5}{x^2 y^2} \\ P_0(E_\gamma) &\propto \frac{1 + (1 - E_\gamma/(E_e - E_\gamma))^2}{E_\gamma/(E_e - E_\gamma)}\,. \end{aligned}$$

The probability density $P(\vec{D}|x, y, E_\gamma)$ was calculated using parametrisations of the resolutions as found from MC studies. The quantities (x, y, E_γ) at the global mode of the

posterior were used to extract the kinematic-fit values for the energies and angles of the electron and hadronic system. The pulls were defined as the difference between the measured value and the fitted value, divided by the RMS extracted from the MC. Studies of these pull distributions allowed the determination of biases between the MC and the data, the variation of which were used to set limits on the systematic uncertainties.

As an example, the pull distributions for data and MC are shown in Fig. 2 for the e^+p sample for the different quantities entering the fit. Excellent agreement is found between data and simulation. Similarly, excellent agreement is observed for the e^-p sample (not shown).

6 Event selection

6.1 Trigger

ZEUS operated a three-level trigger system [10, 37, 38]. At the first level, only coarse calorimeter and tracking information was available. Events were selected using criteria based on an energy deposit in the CAL consistent with an isolated electron candidate. In addition, events with high transverse energy in coincidence with a CTD track were accepted. At the second level, the value of

$$\delta \equiv \sum_i (E - p_Z)_i = \sum_i (E_i - E_i \cos\theta_i) \ , \tag{7}$$

where the sum runs over all calorimeter energy deposits E_i with polar angles θ_i, was required to be higher than 29 GeV to ensure efficient selection of NC events, for which $\delta = 2E_e$ is expected when no detector effects are present. Timing information from the calorimeter was used to reject events inconsistent with the bunch-crossing time. At the third level, events were fully reconstructed and selected according to requirements similar to, but looser than, the offline cuts described below.

6.2 Offline event selection

Offline, events were selected according to the following criteria:

- a scattered electron candidate with $E_e^{'} > 15$ GeV was required. A track matched to the energy deposit in the calorimeter was required for events in which the electron was found within the acceptance of the tracking detectors. This was done by requiring the distance of closest approach (DCA) between the track extrapolated to the calorimeter surface and the position of the energy cluster to be less than 10 cm and the electron

track momentum, p_e, to be larger than 5 GeV. A matched track was not required if the electron emerged in the FCAL with a polar angle outside the acceptance of the CTD. In this case, it was required to have $p_T^e > 30\,\text{GeV}$. An isolation requirement was imposed such that the energy not associated with the electron in an $\eta - \phi$-cone of radius 0.8 centred on the electron was less than 4 GeV;

- fiducial-volume cuts were applied to the position of the scattered-electron candidate to ensure that it was within a region in which the experimental resolution is well understood. A cut excluded the electron candidates in the transition region between FCAL and BCAL ($0.52 < \theta < 0.65$). Events for which the Z position of the electron in the CAL $Z_e < -95\,\text{cm}$ were also excluded, as well as electrons in the BCAL within 1.4 cm of the module gap or 0.6 cm of the cell gap;
- up to three jets were allowed. Valid jets were required to have $E_T^{\text{jet}} > 10\,\text{GeV}$ and their reconstructed position had to be outside a box of $40{\times}40$ cm^2 around the FCAL beam pipe.

The following set of cuts was applied to remove background events:

- the value $\delta > 40\,\text{GeV}$ was used to remove NC events with hard QED intial-state radiation and to reject photoproduction events (events in which the scattered electron escapes through the rear beam hole). In addition, $\delta < 65\,\text{GeV}$ was required to remove events in which a normal DIS event coincided with additional energy deposits in the RCAL from beam-gas interactions. To remove residual photoproduction background, y calculated from the electron-candidate variables was required to be less than 0.8;
- to remove non-ep background, events were required to have a reconstructed vertex within the range $-50 < Z_{\text{vtx}} < 50\,\text{cm}$;
- the net transverse momentum is expected to be small for NC events. To remove cosmic-ray events and beam-related background events, the quantity $P_T/\sqrt{E_T}$ was required to be less than $4\sqrt{\text{GeV}}$. The variables P_T and E_T are defined by

$$\begin{aligned} P_T^2 &= P_X^2 + P_Y^2 = \left(\sum_i E_i \sin\theta_i \cos\phi_i\right)^2 + \left(\sum_i E_i \sin\theta_i \sin\phi_i\right)^2, \\ E_T &= \sum_i E_i \sin\theta_i, \end{aligned}$$

  where the sums run over all calorimeter energy deposits, E_i, with polar and azimuthal angles θ_i and ϕ_i with respect to the event vertex, respectively;
- to ensure that zero-jet events originate from a large-x scattering, a limit was imposed on y_{JB} such that $y_{\text{JB}} < 1.3 \cdot Q^2_{\text{edge}}/(s \cdot x_{\text{edge}})$, where x_{edge} and Q^2_{edge} are the lower x and upper Q^2 edges of the bins defined for the integrated-cross-section measurements up to $x = 1$.

The number of events remaining after all these selection cuts were 53 099 for the e^-p and 37 361 for the e^+p sample, of which 1 877 and 1 325 were found with zero jets, respectively.

7 Data and MC comparison

The MC simulation was used to correct for detector acceptance, trigger and offline selection efficiencies and for smearing effects due to finite resolution. Given that the measured distributions are steep functions of x and Q^2, it is very important to have a good description of the underlying physics distributions and a good understanding of the resolution effects.

7.1 Treatment of the hadronic final state

In order to assess the quality of modelling of the hadronic final state, a detailed comparison of the data and the MC was performed in distributions such as the jet multiplicity, $N_{\rm jet}$, jet transverse energy, $E_T^{\rm jet}$, and the polar angle of the jets, $\theta_{\rm jet}$. While the ARIADNE MC gave a better description of the $E_T^{\rm jet}$ distribution, LEPTO gave a better description of the $N_{\rm jet}$ distribution. Since both MC sets have identical generated x and Q^2 distributions, a linear mixture of the two could be constructed,

$$N_{\rm MC}(x,Q^2) = \lambda \cdot N_{\rm Ariadne}(x,Q^2) + (1-\lambda) \cdot N_{\rm Lepto}(x,Q^2)\,, \tag{8}$$

where N denotes the number of generated events in a given x and Q^2 bin and the subscripts denote the MC samples. The fraction λ was determined by fitting the 3-dimensional distribution in $N_{\rm jet}$, $E_T^{\rm jet}$ and $\theta_{\rm jet}$ in the data. The best fit to the combined e^-p and e^+p data samples was obtained with $\lambda = 0.3$ with a systematic uncertainty of 0.3. It was further checked that the description of the data improves for all relevant distributions, not only for those which were used in the fit. A comparison between data distributions and MC expectations with $\lambda = 0.3$ for electron and jet variables is shown for events with $Q^2 > 550\,{\rm GeV}^2$ and $y < 0.8$, for the e^-p sample in Fig. 3 and for the e^+p sample in Fig. 4. The comparison between the distributions of Q^2, $N_{\rm jet}$ and x for events with at least one reconstructed jet is shown in Fig. 5. Very good agreement is achieved in all distributions. Subsequent comparisons use the linear combination of ARIADNE and LEPTO with $\lambda = 0.3$, which is denoted simply as 'MC'.

8 Cross-section determination

The bin widths in the (x, Q^2)-plane are chosen to be sufficiently large compared to the resolution of the variables being measured so that the migrations between neighbouring bins are acceptable. The $x_{\rm edge}$, the lower x edge of the zero-jet bin, was determined using $\theta_{\rm jet} = 0.11$ rad. The efficiency, defined as the number of events generated and reconstructed in a given bin after all selection cuts divided by the number of events generated in that bin, was typically 50%, mainly driven by geometrical fiducial cuts. The efficiency was lower in low-Q^2 bins due to removal of electrons in RCAL and in the B/RCAL transition region. The purity, which is defined as the number of events reconstructed and generated in a particular bin after all selection cuts divided by the number of events reconstructed in that bin, was typically 60%.

The double-differential cross section in bins of Q^2 and x was determined as follows:

$$\frac{d^2\sigma(x,Q^2)}{dxdQ^2} = \frac{N_{\rm data}(\Delta x, \Delta Q^2)}{N_{\rm MC}(\Delta x, \Delta Q^2)} \frac{d^2\sigma^{\rm SM}_{\rm Born}(x,Q^2)}{dxdQ^2}, \tag{9}$$

and the integrated cross section was determined as

$$\int\limits_{x_{\rm edge}}^{1} \frac{d^2\sigma(x,Q^2)}{dxdQ^2}dx = \frac{N_{\rm data}(\Delta x, \Delta Q^2)}{N_{\rm MC}(\Delta x, \Delta Q^2)} \int\limits_{x_{\rm edge}}^{1} \frac{d^2\sigma^{\rm SM}_{\rm Born}(x,Q^2)}{dxdQ^2}dx, \tag{10}$$

where $N_{\rm data}(\Delta x, \Delta Q^2)$ is the number of data events reconstructed in a bin $(\Delta x, \Delta Q^2)$ and $N_{\rm MC}(\Delta x, \Delta Q^2)$ is the corresponding number of simulated events normalised to the data luminosity. The SM prediction, $d^2\sigma^{\rm SM}_{\rm Born}(x,Q^2)/dxdQ^2$, was evaluated according to Eq. (1) with the same PDF and electroweak parameters as used in the MC simulation. This procedure implicitly takes into account the acceptance, bin-centring and leading-order electroweak radiative corrections from the MC simulation.

9 Systematic uncertainties

The systematic effects related to the uncertainties in the MC simulation were estimated by recalculating the cross section for variations of the parameters by their uncertainties (see Section 5). The positive and negative deviations from the nominal cross section were added separately in quadrature to obtain the total positive and negative systematic uncertainty.

9.1 Uncorrelated systematic uncertainties

The following systematic uncertainties are either small or exhibit no bin-to-bin correlations:

- electron-energy resolution – the effect on the value of the cross section of changing the resolution of the electron energy measured in the calorimeter by $\pm 3\%$ was less than 1.5% for almost all bins;
- electron-isolation requirement – variation of the electron-isolation energy by $\pm 2\,\mathrm{GeV}$ caused the cross section to vary within 1.5% for most of the bins, rising to a maximum of 3% for a few bins;
- track-matching efficiency – this correction was varied within the limits allowed by its statistical uncertainty; the resulting variation in the cross section was found to be less than 0.2% for all bins;
- FCAL alignment – the position of the jet on the face of the FCAL was varied by $\pm 5\,\mathrm{mm}$ in both the X and the Y direction. The resulting changes in the cross sections were negligible in low-Q^2 bins, rising to a maximum of 5% in high-Q^2 bins;
- BCAL alignment – the position of the electron on the face of the CAL along Z and along the azimuthal direction was varied by ± 1 mm, respectively. The resulting changes in the cross sections were negligible;
- F/BCAL crack cut – the cut on the electron polar angle in this region was varied by $\pm 15\,\mathrm{mrad}$ and the resulting variation in the cross section was found to be negligible for almost all bins, except a few high-Q^2 bins, where the variation increased to 5%;
- background – the estimated background from all sources was less than 0.015% and therefore the associated contribution and systematic uncertainty were neglected.

9.2 Correlated systematic uncertainties

The significant correlated systematic uncertainties are listed below and labelled for further reference as follows:

- $\{\delta_1\}$ electron-energy scale – the systematic uncertainty resulting from variation of the electron-energy scale by 0.5% resulted in typically less than 3% variation in cross sections for almost all bins, except for some bins at high Q^2, where this value rose to 10%;
- $\{\delta_2\}$ jet-energy scale – the uncertainty in the cross-section measurement due to variation of the jet-energy scale by 1% had a negligible effect for almost all bins and was well within 1%;

- $\{\delta_3\}$ simulation of the hadronic final state – the analysis was repeated while varying the relative contribution of ARIADNE and LEPTO MEPS by ± 0.3. The resulting uncertainty was well within 2% for low-Q^2 bins, increasing to 10% for the highest-x bins at high Q^2;
- $\{\delta_4\}$ PDF uncertainties – the MCs were reweighted to variants of HERAPDF1.5, representing the PDF uncertainties that were found to lead to the largest deviations from the central PDF set expectations for the NC cross sections. The resulting systematic uncertainties are very small with the exceptions of the highest Q^2 and x bins, where the uncertainty reaches 3%.

In addition, there is a global uncertainty due to the luminosity measurement of 1.8%.

10 Results

The measured double-differential Born-level cross section as a function of Q^2 and x is presented in Tables 1 and 2, for e^-p and e^+p scattering, respectively. For the highest integrated x bin, the respective average cross sections, defined as

$$I(x) = \frac{1}{1 - x_{\text{edge}}} \int_{x_{\text{edge}}}^{1} \frac{d^2\sigma(x, Q^2)}{dx dQ^2} dx \ , \tag{11}$$

are presented in Tables 3 and 4 as a function of Q^2. Also listed are the statistical and systematic uncertainties. The latter are given separately for the quadratically summed uncorrelated and correlated uncertainties. For bins populated by fewer than 50 events, the statistical uncertainties are quoted as the central 68% probability interval calculated using the prior of Jeffreys [39].

The results are presented in Figs. 6 and 7. The averaged integrated cross sections are plotted at $x = (x_{\text{edge}}+1)/2$. The measurements are compared to SM expectations obtained with the HERAPDF 1.5 PDFs [22]. Within the quoted uncertainties, with statistical and systematic uncertainties added in quadrature, the agreement between measurements and expectations is good.

The ratio of the measured cross sections to those expected from HERAPDF1.5 are shown in Figs. 8 and 9. Note that for bins where no events are observed, the limit is quoted at 68% probability, neglecting the systematic uncertainty. Also shown are the predictions from a number of other PDF sets (ABM11 [40], CT10 [41], MSTW2008 [42], NNPDF2.3 [43]), normalised to the predictions from HERAPDF1.5. Within the quoted uncertainties, the agreement between measurements and expectations is good.

The measurement presented here is based on the same data set used for previous ZEUS publications [6, 7]. The advantage of the present measurements is a finer binning in x and an extension of the kinematic coverage up to $x \cong 1$. In the region of $Q^2 \geq 725\,\mathrm{GeV}^2$ and $y < 0.8$, the cross sections presented here could replace those previously published to assess their impact on the PDFs at high x, where little data is available.

11 Summary

Neutral current e^-p and e^+p DIS cross sections have been measured in the ZEUS detector as a function of x and Q^2 for $Q^2 \geq 725\,\mathrm{GeV}^2$ and up to $x \cong 1$. The novel reconstruction method and the large volume of data available allowed a high precision, limited only by statistical uncertainties, to be achieved. The results are in good agreement with SM predictions from HERAPDF1.5 and several other commonly used sets of PDFs. The fine binning in x, the extension of the kinematic coverage up to $x \cong 1$ and the excellent control of the systematic uncertainties make these data an important input to fits constraining the PDFs in the valence-quark domain in a model-independent way.

Acknowledgements

We appreciate the contributions to the construction, maintenance and operation of the ZEUS detector made by many people who are not listed as authors. The HERA machine group and the DESY computing staff are especially acknowledged for their success in providing excellent operation of the collider and the data-analysis environment. We thank the DESY directorate for their strong support and encouragement.

References

[1] H1 and ZEUS Coll., F.D. Aaron et al., JHEP **1001**, 109 (2010).

[2] BCDMS Coll., A.C. Benvenuti et al., Phys. Lett. **B 223**, 485 (1989).

[3] L.W. Whitlow et al., Phys. Lett. **B 282**, 475 (1992).

[4] S.J. Brodsky and G.R. Farrar, Phys. Rev. Lett. **31**, 1153 (1973).

[5] ZEUS Coll., S. Chekanov et al., Eur. Phys. J. **C 49**, 523 (2007).

[6] ZEUS Coll., S. Chekanov et al., Eur. Phys. J. **C 62**, 625 (2009).

[7] ZEUS Coll., H. Abramowicz et al., Phys. Rev. **D 87**, 052014 (2013).

[8] R. Devenish and A. Cooper-Sarkar, *Deep Inelastic Scattering*, Oxford University Press, 2003.

[9] M. Klein and T. Riemann, Z. Phys. **C 24**, 151 (1984).

[10] ZEUS Coll., U. Holm (ed.), *The ZEUS Detector.* Status report (unpublished), DESY (1993), available on http://www-zeus.desy.de/bluebook/bluebook.html.

[11] N. Harnew et al., Nucl. Inst. Meth. **A 279**, 290 (1989);
B. Foster et al., Nucl. Phys. Proc. Suppl. **B 32**, 181 (1993);
B. Foster et al., Nucl. Inst. Meth. **A 338**, 254 (1994).

[12] A. Polini et al., Nucl. Inst. Meth. **A 581**, 656 (2007).

[13] S. Fourletov, Nucl. Inst. Meth. **A 535**, 191 (2004).

[14] M. Derrick et al., Nucl. Inst. Meth. **A 309**, 77 (1991);
A. Andresen et al., Nucl. Inst. Meth. **A 309**, 101 (1991);
A. Caldwell et al., Nucl. Inst. Meth. **A 321**, 356 (1992);
A. Bernstein et al., Nucl. Inst. Meth. **A 336**, 23 (1993).

[15] J. Andruszkow et al., *First measurement of HERA luminosity by ZEUS lumi monitor*, DESY-92-066 (1992);
ZEUS Coll., M. Derrick et al., Z. Phys. **C 63**, 391 (1994);
J. Andruszkow et al., Acta Phys. Pol. **B 32**, 2025 (2001).

[16] M. Helbich et al., Nucl. Inst. Meth. **A 565**, 572 (2006).

[17] J. Böhme, Eur. Phys. J. **C 33**, 1067 (2004).

[18] D.P. Barber et al., Nucl. Inst. Meth. **A 329**, 79 (1993).

[19] M. Beckmann et al., Nucl. Inst. Meth. **A 479**, 334 (2002).

[20] A. Kwiatkowski, H. Spiesberger and H.-J. Möhring, Comp. Phys. Comm. **69**, 155 (1992). Also in *Proc. Workshop Physics at HERA*. eds. W. Buchmüller and G. Ingelman, (DESY, Hamburg, 1991).

[21] H. Spiesberger, HERACLES and DJANGOH: *Event Generation for ep Interactions at HERA Including Radiative Processes*, 1998, available on http://www.desy.de/ hspiesb/djangoh.html.

[22] V. Radescu, *Combination of QCD Analysis of the HERA Inclusive Cross Sections*, arXiv: 1308.0374 [hep-ex] (2013).

[23] G. Ingelman, A. Edin and J. Rathsman, Comp. Phys. Comm. **101**, 108 (1997).

[24] L. Lönnblad, Comp. Phys. Comm. **71**, 15 (1992).

[25] T. Sjöstrand, Comp. Phys. Comm. **39**, 347 (1986).

[26] G. Marchesini et al., Comp. Phys. Comm. **67**, 465 (1992).

[27] T. Abe, Comp. Phys. Comm. **136**, 126 (2001).

[28] R. Brun et al., GEANT3, Technical Report CERN-DD/EE/84-1, CERN (1987).

[29] ZEUS Coll., S. Chekanov et al., Eur. Phys. J. **C 28**, 175 (2003).

[30] ZEUS Coll., J. Breitweg et al., Eur. Phys. J. **C 11**, 427 (1999).

[31] F. Jacquet and A. Blondel, *Proc. the Study of an ep Facility for Europe*, U. Amaldi (ed.), p. 391 (1997). Also in DESY 79-48 (1997).

[32] S. Catani et al., Nucl. Phys. **B 406**, 187 (1993).

[33] G. Briskin, PhD Thesis, Tel Aviv University, DESY-THESIS 1998-036 (1998).

[34] J.E. Huth et al., *Toward a standardization of jet definitions, Research Directions for the Decade. Proceedings of Summer Study on High Energy Physics, 1990*, E.L. Berger (ed.), p. 134. World Scientific (1992) Also in FERMILAB-CONF-90-249-E.

[35] A. Caldwell, D. Kollar and K. Kroninger, Comp. Phys. Comm. **180**, 2197 (2009).

[36] R. Aggarwal, PhD Thesis, Panjab University, (2013).

[37] W.H. Smith, K. Tokushuku and L.W. Wiggers, *Proc. Computing in High-Energy Physics (CHEP), Annecy, France, Sept. 1992*, C. Verkek and W. Wojcik (eds.), p. 222, CERN, Geneva, Switzerland (1992).Also in DESY 92-150B (1992).

[38] P.D. Allfrey et al., Nucl. Inst. Meth. **A 580**, 1257 (2007).

[39] H. Jeffreys, Proceedings of the Royal Society of London, Series A, Math. and Phys. Sci. **186**, 453 (1946).

[40] S. Alekhin, J. Blümlein and S.O. Moch, PoS **LL2012**, 016 (2012).

[41] M. Guzzi et al., *CT10 parton distributions and other developments in the global QCD analysis*, SMU-HEP-10-11 (2011), arXiv: 1101.0561 [hep-ph] (2011).

[42] A.D. Martin et al., Eur. Phys. J. **C 63**, 189 (2009).

[43] R. Ball et al., JHEP **1304**, 125 (2013).

Q^2 (GeV^2)	x	N	$d^2\sigma/dxdQ^2$ (pb/GeV^2)	$\delta_{\rm stat}$ (%)	$\delta_{\rm sys}$ (%)	$\delta_{\rm u}$ (%)	δ_1 (%)	δ_2 (%)	δ_3 (%)	δ_4 (%)
725	0.06	743	$3.39e+00$	$^{+3.7}_{-3.7}$	$^{+2.1}_{-1.8}$	$^{+1.2}_{-1.2}$	$^{+0.8}_{-0.2}$	$^{-0.2}_{+0.1}$	$^{+1.4}_{-1.4}$	$^{+0.1}_{-0.1}$
725	0.08	580	$2.63e+00$	$^{+4.2}_{-4.2}$	$^{+1.5}_{-2.3}$	$^{+1.3}_{-1.5}$	$^{+0.7}_{-1.7}$	$^{-0.2}_{+0.0}$	$^{-0.1}_{+0.1}$	$^{+0.1}_{-0.1}$
725	0.10	441	$1.89e+00$	$^{+4.8}_{-4.8}$	$^{+1.5}_{-1.6}$	$^{+1.5}_{-1.5}$	$^{+0.2}_{-0.4}$	$^{+0.0}_{+0.1}$	$^{+0.2}_{-0.2}$	$^{+0.1}_{-0.1}$
725	0.12	416	$1.45e+00$	$^{+4.9}_{-4.9}$	$^{+3.2}_{-2.3}$	$^{+1.6}_{-1.6}$	$^{+2.1}_{-1.6}$	$^{-0.1}_{+0.0}$	$^{+0.5}_{-0.5}$	$^{+0.1}_{-0.1}$
725	0.16	283	$1.05e+00$	$^{+5.9}_{-5.9}$	$^{+2.6}_{-2.8}$	$^{+1.9}_{-2.1}$	$^{+1.4}_{-1.3}$	$^{-0.0}_{+0.2}$	$^{+0.4}_{-0.4}$	$^{+0.1}_{-0.1}$
725	0.19	248	$7.18e-01$	$^{+6.3}_{-6.3}$	$^{+2.7}_{-2.9}$	$^{+1.9}_{-1.9}$	$^{+1.7}_{-1.8}$	$^{-0.1}_{-0.2}$	$^{+0.3}_{-0.3}$	$^{+0.1}_{-0.1}$
725	0.23	227	$5.88e-01$	$^{+6.6}_{-6.6}$	$^{+2.4}_{-2.3}$	$^{+2.1}_{-2.2}$	$^{+1.1}_{-0.6}$	$^{+0.1}_{+0.1}$	$^{-0.4}_{+0.4}$	$^{+0.1}_{-0.1}$
875	0.05	789	$2.86e+00$	$^{+3.6}_{-3.6}$	$^{+1.1}_{-1.2}$	$^{+1.1}_{-1.2}$	$^{-0.3}_{+0.2}$	$^{-0.2}_{+0.2}$	$^{+0.1}_{-0.1}$	$^{+0.1}_{-0.1}$
875	0.07	681	$2.05e+00$	$^{+3.8}_{-3.8}$	$^{+1.2}_{-1.4}$	$^{+1.1}_{-1.2}$	$^{-0.3}_{+0.2}$	$^{-0.1}_{+0.2}$	$^{-0.3}_{+0.3}$	$^{+0.1}_{-0.1}$
875	0.09	604	$1.62e+00$	$^{+4.1}_{-4.1}$	$^{+1.4}_{-1.7}$	$^{+1.4}_{-1.4}$	$^{-0.3}_{+0.1}$	$^{-0.1}_{+0.1}$	$^{-0.4}_{+0.4}$	$^{+0.1}_{-0.1}$
875	0.11	493	$1.16e+00$	$^{+4.5}_{-4.5}$	$^{+1.7}_{-1.4}$	$^{+1.5}_{-1.4}$	$^{+0.4}_{+0.4}$	$^{+0.1}_{+0.1}$	$^{-0.1}_{+0.1}$	$^{+0.1}_{-0.1}$
875	0.14	403	$8.33e-01$	$^{+5.0}_{-5.0}$	$^{+1.7}_{-2.2}$	$^{+1.5}_{-1.6}$	$^{-0.7}_{-0.4}$	$^{-0.2}_{+0.0}$	$^{+0.8}_{-0.8}$	$^{+0.1}_{-0.1}$
875	0.17	385	$6.13e-01$	$^{+5.1}_{-5.1}$	$^{+2.2}_{-2.0}$	$^{+1.8}_{-1.8}$	$^{-0.2}_{+0.2}$	$^{-0.2}_{+0.1}$	$^{+0.9}_{-0.9}$	$^{+0.1}_{-0.1}$
875	0.21	271	$4.33e-01$	$^{+6.1}_{-6.1}$	$^{+2.0}_{-2.4}$	$^{+1.8}_{-2.4}$	$^{-0.5}_{-0.0}$	$^{-0.0}_{-0.1}$	$^{+0.8}_{-0.8}$	$^{+0.0}_{-0.0}$
875	0.25	258	$3.47e-01$	$^{+6.2}_{-6.2}$	$^{+2.7}_{-2.4}$	$^{+2.0}_{-2.0}$	$^{-0.4}_{+0.5}$	$^{+0.0}_{-0.0}$	$^{-0.5}_{+0.5}$	$^{+0.0}_{-0.0}$
1025	0.05	598	$2.14e+00$	$^{+4.1}_{-4.1}$	$^{+1.5}_{-1.9}$	$^{+1.3}_{-1.3}$	$^{-1.1}_{+0.1}$	$^{-0.2}_{+0.1}$	$^{+0.6}_{-0.6}$	$^{+0.1}_{-0.1}$
1025	0.07	489	$1.46e+00$	$^{+4.5}_{-4.5}$	$^{+2.2}_{-1.7}$	$^{+1.4}_{-1.4}$	$^{-0.6}_{+1.2}$	$^{-0.2}_{+0.3}$	$^{+0.3}_{-0.3}$	$^{+0.1}_{-0.1}$
1025	0.09	450	$1.11e+00$	$^{+4.7}_{-4.7}$	$^{+1.9}_{-2.0}$	$^{+1.4}_{-1.5}$	$^{-0.6}_{+1.0}$	$^{-0.0}_{+0.1}$	$^{+0.5}_{-0.5}$	$^{+0.1}_{-0.1}$
1025	0.11	402	$8.58e-01$	$^{+5.0}_{-5.0}$	$^{+2.0}_{-2.5}$	$^{+1.5}_{-1.5}$	$^{-1.4}_{+0.7}$	$^{+0.2}_{+0.1}$	$^{+0.7}_{-0.7}$	$^{+0.1}_{-0.1}$
1025	0.14	342	$6.18e-01$	$^{+5.4}_{-5.4}$	$^{+2.1}_{-1.8}$	$^{+1.7}_{-1.7}$	$^{-0.3}_{+1.2}$	$^{-0.4}_{-0.1}$	$^{-0.3}_{+0.3}$	$^{+0.1}_{-0.1}$
1025	0.17	231	$4.39e-01$	$^{+6.6}_{-6.6}$	$^{+2.4}_{-1.9}$	$^{+1.9}_{-1.9}$	$^{+0.6}_{+0.1}$	$^{-0.1}_{+0.2}$	$^{-0.2}_{+0.2}$	$^{+0.1}_{-0.1}$
1025	0.20	224	$3.13e-01$	$^{+6.7}_{-6.7}$	$^{+2.7}_{-3.6}$	$^{+2.1}_{-2.2}$	$^{-1.9}_{+0.5}$	$^{-0.0}_{-0.1}$	$^{-1.6}_{+1.6}$	$^{+0.0}_{-0.0}$
1025	0.27	363	$2.12e-01$	$^{+5.2}_{-5.2}$	$^{+2.5}_{-2.5}$	$^{+1.6}_{-1.7}$	$^{-0.7}_{+1.0}$	$^{-0.0}_{+0.1}$	$^{+1.4}_{-1.4}$	$^{+0.0}_{-0.0}$

Table 1: The double-differential cross section, $d^2\sigma/dxdQ^2$, for NC e^-p scattering at $\sqrt{s} = 318\,\text{GeV}$ as a function of Q^2 and x. Also quoted are the number of events reconstructed and selected in the bin, N, the statistical uncertainty, $\delta_{\rm stat}$, the total systematic uncertainty, $\delta_{\rm sys}$, the total uncorrelated systematic uncertainty, $\delta_{\rm u}$, followed by the bin-to-bin correlated systematic uncertainties, δ_1–δ_4, defined in Section 9. The luminosity uncertainty of 1.8% is not included. This table has five continuations.

Q^2 (GeV^2)	x	N	$d^2\sigma/dxdQ^2$ (pb/GeV^2)	$\delta_{\rm stat}$ (%)	$\delta_{\rm sys}$ (%)	$\delta_{\rm u}$ (%)	δ_1 (%)	δ_2 (%)	δ_3 (%)	δ_4 (%)
1200	0.06	552	$1.46e+00$	$^{+4.3}_{-4.3}$	$^{+1.7}_{-1.9}$	$^{+1.4}_{-1.4}$	$^{-0.9}_{+0.6}$	$^{-0.3}_{+0.4}$	$^{-0.2}_{+0.2}$	$^{+0.1}_{-0.1}$
1200	0.07	454	$1.02e+00$	$^{+4.7}_{-4.7}$	$^{+1.5}_{-1.8}$	$^{+1.4}_{-1.4}$	$^{-0.7}_{+0.2}$	$^{-0.1}_{-0.0}$	$^{+0.2}_{-0.2}$	$^{+0.1}_{-0.1}$
1200	0.09	412	$7.52e-01$	$^{+4.9}_{-4.9}$	$^{+1.9}_{-2.2}$	$^{+1.5}_{-1.5}$	$^{-0.7}_{+1.1}$	$^{-0.3}_{+0.0}$	$^{+0.1}_{-0.1}$	$^{+0.1}_{-0.1}$
1200	0.12	430	$5.39e-01$	$^{+4.8}_{-4.8}$	$^{+2.3}_{-2.3}$	$^{+1.5}_{-1.4}$	$^{-1.1}_{+0.9}$	$^{-0.1}_{+0.1}$	$^{+1.0}_{-1.0}$	$^{+0.1}_{-0.1}$
1200	0.14	326	$4.22e-01$	$^{+5.5}_{-5.5}$	$^{+2.4}_{-1.8}$	$^{+1.9}_{-1.7}$	$^{-0.3}_{+1.2}$	$^{+0.0}_{+0.1}$	$^{-0.3}_{+0.3}$	$^{+0.1}_{-0.1}$
1200	0.18	272	$2.80e-01$	$^{+6.1}_{-6.1}$	$^{+2.1}_{-2.6}$	$^{+1.9}_{-1.9}$	$^{-1.0}_{+0.7}$	$^{-0.1}_{+0.0}$	$^{+0.5}_{-0.5}$	$^{+0.0}_{-0.0}$
1200	0.22	209	$2.13e-01$	$^{+6.9}_{-6.9}$	$^{+2.8}_{-2.6}$	$^{+2.1}_{-2.1}$	$^{-1.3}_{+1.4}$	$^{-0.1}_{+0.2}$	$^{-0.5}_{+0.5}$	$^{+0.0}_{-0.0}$
1200	0.29	310	$1.30e-01$	$^{+5.7}_{-5.7}$	$^{+2.5}_{-2.6}$	$^{+1.7}_{-1.7}$	$^{-1.7}_{+1.2}$	$^{-0.0}_{+0.0}$	$^{-0.2}_{+0.2}$	$^{+0.0}_{-0.0}$
1400	0.06	358	$8.78e-01$	$^{+5.3}_{-5.3}$	$^{+1.7}_{-2.3}$	$^{+1.6}_{-1.7}$	$^{-1.1}_{+0.7}$	$^{-0.3}_{+0.0}$	$^{-0.1}_{+0.1}$	$^{+0.1}_{-0.1}$
1400	0.08	308	$6.45e-01$	$^{+5.7}_{-5.7}$	$^{+2.0}_{-1.9}$	$^{+1.7}_{-1.7}$	$^{-0.6}_{+0.8}$	$^{-0.1}_{+0.2}$	$^{+0.1}_{-0.1}$	$^{+0.1}_{-0.1}$
1400	0.10	317	$5.25e-01$	$^{+5.6}_{-5.6}$	$^{+2.0}_{-2.1}$	$^{+1.8}_{-1.8}$	$^{-0.9}_{+0.7}$	$^{-0.1}_{+0.0}$	$^{+0.0}_{-0.0}$	$^{+0.1}_{-0.1}$
1400	0.12	300	$3.76e-01$	$^{+5.8}_{-5.8}$	$^{+2.1}_{-2.2}$	$^{+1.8}_{-1.8}$	$^{-1.0}_{+0.7}$	$^{-0.1}_{+0.1}$	$^{-0.5}_{+0.5}$	$^{+0.1}_{-0.1}$
1400	0.16	206	$2.68e-01$	$^{+7.0}_{-7.0}$	$^{+2.2}_{-2.2}$	$^{+2.1}_{-2.2}$	$^{-0.4}_{+0.4}$	$^{-0.1}_{+0.1}$	$^{-0.1}_{+0.1}$	$^{+0.0}_{-0.0}$
1400	0.19	183	$1.83e-01$	$^{+7.4}_{-7.4}$	$^{+2.4}_{-2.2}$	$^{+2.1}_{-2.1}$	$^{-0.5}_{+0.9}$	$^{-0.0}_{+0.2}$	$^{+0.3}_{-0.3}$	$^{+0.0}_{-0.0}$
1400	0.23	139	$1.39e-01$	$^{+8.5}_{-8.5}$	$^{+2.5}_{-2.8}$	$^{+2.5}_{-2.5}$	$^{-0.9}_{-0.1}$	$^{-0.2}_{+0.1}$	$^{-0.5}_{+0.5}$	$^{+0.0}_{-0.0}$
1400	0.31	231	$8.58e-02$	$^{+6.6}_{-6.6}$	$^{+2.9}_{-2.4}$	$^{+2.0}_{-2.0}$	$^{-1.1}_{+1.7}$	$^{-0.0}_{-0.0}$	$^{-0.4}_{+0.4}$	$^{+0.0}_{-0.0}$
1650	0.05	419	$7.18e-01$	$^{+4.9}_{-4.9}$	$^{+1.8}_{-1.9}$	$^{+1.5}_{-1.5}$	$^{-1.0}_{+0.7}$	$^{-0.4}_{+0.2}$	$^{-0.4}_{+0.4}$	$^{+0.0}_{-0.0}$
1650	0.07	358	$5.44e-01$	$^{+5.3}_{-5.3}$	$^{+2.3}_{-2.0}$	$^{+1.7}_{-1.6}$	$^{-0.8}_{+1.0}$	$^{-0.1}_{+0.2}$	$^{+0.2}_{-0.2}$	$^{+0.0}_{-0.0}$
1650	0.09	351	$4.32e-01$	$^{+5.3}_{-5.3}$	$^{+2.0}_{-1.7}$	$^{+1.6}_{-1.6}$	$^{-0.3}_{+0.7}$	$^{-0.3}_{+0.2}$	$^{-0.2}_{+0.2}$	$^{+0.1}_{-0.1}$
1650	0.11	298	$2.98e-01$	$^{+5.8}_{-5.8}$	$^{+2.2}_{-2.0}$	$^{+1.7}_{-1.7}$	$^{-0.7}_{+0.9}$	$^{-0.1}_{+0.2}$	$^{+0.4}_{-0.4}$	$^{+0.1}_{-0.1}$
1650	0.14	276	$2.22e-01$	$^{+6.0}_{-6.0}$	$^{+2.0}_{-2.1}$	$^{+1.9}_{-1.8}$	$^{-0.8}_{+0.6}$	$^{-0.1}_{+0.1}$	$^{+0.2}_{-0.2}$	$^{+0.0}_{-0.0}$
1650	0.17	254	$1.62e-01$	$^{+6.3}_{-6.3}$	$^{+2.2}_{-2.2}$	$^{+1.9}_{-1.9}$	$^{-0.7}_{+0.8}$	$^{-0.2}_{+0.1}$	$^{+0.6}_{-0.6}$	$^{+0.0}_{-0.0}$
1650	0.21	195	$1.30e-01$	$^{+7.2}_{-7.2}$	$^{+2.8}_{-2.4}$	$^{+2.2}_{-2.2}$	$^{-0.7}_{+1.4}$	$^{-0.1}_{+0.1}$	$^{+0.1}_{-0.1}$	$^{+0.0}_{-0.0}$
1650	0.25	158	$8.26e-02$	$^{+8.0}_{-8.0}$	$^{+2.6}_{-2.7}$	$^{+2.4}_{-2.3}$	$^{-0.8}_{+0.9}$	$^{-0.2}_{+0.1}$	$^{+0.3}_{-0.3}$	$^{+0.0}_{-0.0}$
1650	0.34	227	$5.61e-02$	$^{+6.6}_{-6.6}$	$^{+2.9}_{-2.9}$	$^{+2.1}_{-2.2}$	$^{-1.4}_{+1.5}$	$^{-0.0}_{+0.0}$	$^{-0.9}_{+0.9}$	$^{+0.0}_{-0.0}$

Table 1: Continuation 1.

Q^2 (GeV^2)	x	N	$d^2\sigma/dxdQ^2$ (pb/GeV^2)	$\delta_{\rm stat}$ (%)	$\delta_{\rm sys}$ (%)	$\delta_{\rm u}$ (%)	δ_1 (%)	δ_2 (%)	δ_3 (%)	δ_4 (%)
1950	0.06	265	$4.27e-01$	$^{+6.1}_{-6.1}$	$^{+2.2}_{-2.4}$	$^{+1.9}_{-1.9}$	$^{-1.1}_{+0.8}$	$^{-0.4}_{+0.5}$	$^{+0.4}_{-0.4}$	$^{+0.0}_{-0.0}$
1950	0.08	251	$3.59e-01$	$^{+6.3}_{-6.3}$	$^{+2.4}_{-2.2}$	$^{+2.0}_{-2.0}$	$^{-0.8}_{+0.9}$	$^{-0.2}_{+0.1}$	$^{+0.5}_{-0.5}$	$^{+0.0}_{-0.0}$
1950	0.10	214	$2.36e-01$	$^{+6.8}_{-6.8}$	$^{+2.2}_{-2.4}$	$^{+2.0}_{-2.0}$	$^{-0.8}_{+0.2}$	$^{-0.1}_{+0.2}$	$^{+0.7}_{-0.7}$	$^{+0.0}_{-0.0}$
1950	0.12	228	$1.83e-01$	$^{+6.6}_{-6.6}$	$^{+2.3}_{-2.3}$	$^{+2.1}_{-2.1}$	$^{-0.9}_{+0.8}$	$^{-0.1}_{+0.1}$	$^{+0.3}_{-0.3}$	$^{+0.0}_{-0.0}$
1950	0.16	172	$1.42e-01$	$^{+7.6}_{-7.6}$	$^{+2.6}_{-3.0}$	$^{+2.3}_{-2.5}$	$^{-1.4}_{+0.8}$	$^{-0.3}_{+0.1}$	$^{+0.1}_{-0.1}$	$^{+0.0}_{-0.0}$
1950	0.19	124	$7.81e-02$	$^{+9.0}_{-9.0}$	$^{+3.0}_{-2.4}$	$^{+2.5}_{-2.4}$	$^{-0.3}_{+1.3}$	$^{-0.1}_{+0.1}$	$^{+0.1}_{-0.1}$	$^{+0.0}_{-0.0}$
1950	0.23	157	$8.17e-02$	$^{+8.0}_{-8.0}$	$^{+3.2}_{-2.8}$	$^{+2.6}_{-2.6}$	$^{-0.9}_{+1.5}$	$^{-0.2}_{+0.2}$	$^{-0.3}_{+0.3}$	$^{+0.0}_{-0.0}$
1950	0.28	86	$4.48e-02$	$^{+10.8}_{-10.8}$	$^{+3.2}_{-3.4}$	$^{+3.0}_{-3.1}$	$^{-1.0}_{+0.9}$	$^{-0.0}_{+0.1}$	$^{+0.2}_{-0.2}$	$^{+0.0}_{-0.0}$
1950	0.37	138	$3.06e-02$	$^{+8.5}_{-8.5}$	$^{+3.6}_{-3.8}$	$^{+2.7}_{-2.8}$	$^{-2.1}_{+2.0}$	$^{-0.1}_{+0.0}$	$^{-0.9}_{+0.9}$	$^{+0.0}_{-0.0}$
2250	0.06	214	$3.70e-01$	$^{+6.8}_{-6.8}$	$^{+2.5}_{-2.4}$	$^{+2.1}_{-2.2}$	$^{-0.7}_{+1.1}$	$^{-0.3}_{+0.0}$	$^{-0.3}_{+0.3}$	$^{+0.0}_{-0.0}$
2250	0.07	187	$2.76e-01$	$^{+7.3}_{-7.3}$	$^{+2.5}_{-2.5}$	$^{+2.2}_{-2.3}$	$^{-0.8}_{+0.9}$	$^{-0.0}_{+0.3}$	$^{-0.1}_{+0.1}$	$^{+0.0}_{-0.0}$
2250	0.09	153	$1.93e-01$	$^{+8.1}_{-8.1}$	$^{+2.8}_{-2.6}$	$^{+2.3}_{-2.3}$	$^{-0.2}_{+0.9}$	$^{-0.3}_{+0.5}$	$^{-0.9}_{+0.9}$	$^{+0.0}_{-0.0}$
2250	0.12	159	$1.27e-01$	$^{+7.9}_{-7.9}$	$^{+2.4}_{-2.5}$	$^{+2.2}_{-2.2}$	$^{-1.0}_{+0.5}$	$^{-0.3}_{+0.1}$	$^{-0.2}_{+0.2}$	$^{+0.0}_{-0.0}$
2250	0.14	132	$1.07e-01$	$^{+8.7}_{-8.7}$	$^{+3.0}_{-3.3}$	$^{+2.5}_{-2.6}$	$^{-0.9}_{+1.3}$	$^{-0.1}_{+0.1}$	$^{-0.5}_{+0.5}$	$^{+0.0}_{-0.0}$
2250	0.18	117	$7.29e-02$	$^{+9.2}_{-9.2}$	$^{+2.7}_{-2.7}$	$^{+2.6}_{-2.6}$	$^{-0.5}_{+0.4}$	$^{-0.1}_{+0.1}$	$^{+0.0}_{-0.0}$	$^{+0.0}_{-0.0}$
2250	0.22	75	$4.79e-02$	$^{+11.5}_{-11.5}$	$^{+3.4}_{-3.5}$	$^{+3.3}_{-3.1}$	$^{-1.4}_{+0.5}$	$^{-0.2}_{+0.2}$	$^{-0.4}_{+0.4}$	$^{+0.0}_{-0.0}$
2250	0.26	72	$3.81e-02$	$^{+11.8}_{-11.8}$	$^{+3.7}_{-4.1}$	$^{+3.3}_{-3.3}$	$^{-1.8}_{+1.5}$	$^{-0.1}_{+0.2}$	$^{+0.3}_{-0.3}$	$^{+0.0}_{-0.0}$
2250	0.31	48	$2.48e-02$	$^{+14.4}_{-14.4}$	$^{+4.5}_{-4.2}$	$^{+4.6}_{-3.9}$	$^{-1.6}_{+1.1}$	$^{-0.1}_{+0.1}$	$^{-0.6}_{+0.6}$	$^{+0.0}_{-0.0}$
2250	0.40	76	$1.75e-02$	$^{+11.5}_{-11.5}$	$^{+4.1}_{-4.1}$	$^{+3.6}_{-3.5}$	$^{-1.4}_{+1.3}$	$^{-0.1}_{-0.0}$	$^{+1.3}_{-1.3}$	$^{+0.1}_{-0.1}$
2600	0.09	168	$1.64e-01$	$^{+7.7}_{-7.7}$	$^{+2.5}_{-2.7}$	$^{+2.3}_{-2.4}$	$^{-1.1}_{+0.7}$	$^{-0.3}_{+0.1}$	$^{+0.5}_{-0.5}$	$^{+0.0}_{-0.0}$
2600	0.11	142	$1.06e-01$	$^{+8.4}_{-8.4}$	$^{+2.6}_{-2.6}$	$^{+2.4}_{-2.4}$	$^{-0.6}_{+0.6}$	$^{-0.3}_{+0.3}$	$^{-0.7}_{+0.7}$	$^{+0.0}_{-0.0}$
2600	0.14	160	$9.42e-02$	$^{+7.9}_{-7.9}$	$^{+2.7}_{-2.6}$	$^{+2.4}_{-2.4}$	$^{-0.7}_{+1.1}$	$^{-0.0}_{+0.2}$	$^{+0.2}_{-0.2}$	$^{+0.0}_{-0.0}$
2600	0.17	119	$7.26e-02$	$^{+9.2}_{-9.2}$	$^{+3.0}_{-3.2}$	$^{+2.8}_{-2.9}$	$^{-1.2}_{+1.1}$	$^{-0.2}_{+0.2}$	$^{+0.0}_{-0.0}$	$^{+0.0}_{-0.0}$
2600	0.20	122	$5.69e-02$	$^{+9.1}_{-9.1}$	$^{+3.3}_{-3.1}$	$^{+2.8}_{-2.8}$	$^{-1.0}_{+1.1}$	$^{-0.1}_{+0.2}$	$^{+0.4}_{-0.4}$	$^{+0.0}_{-0.0}$
2600	0.25	111	$4.24e-02$	$^{+9.5}_{-9.5}$	$^{+3.1}_{-3.3}$	$^{+3.0}_{-3.0}$	$^{-1.2}_{+0.5}$	$^{-0.1}_{+0.2}$	$^{+0.3}_{-0.3}$	$^{+0.0}_{-0.0}$
2600	0.29	74	$2.95e-02$	$^{+11.6}_{-11.6}$	$^{+4.1}_{-4.1}$	$^{+3.8}_{-3.8}$	$^{-1.0}_{+1.3}$	$^{-0.2}_{-0.1}$	$^{-0.5}_{+0.5}$	$^{+0.0}_{-0.0}$
2600	0.35	37	$1.17e-02$	$^{+16.4}_{-16.4}$	$^{+4.9}_{-4.1}$	$^{+4.2}_{-4.0}$	$^{-0.8}_{+2.3}$	$^{-0.3}_{+0.1}$	$^{-0.5}_{+0.5}$	$^{+0.0}_{-0.0}$
2600	0.44	67	$1.12e-02$	$^{+12.2}_{-12.2}$	$^{+4.4}_{-4.8}$	$^{+4.0}_{-4.1}$	$^{-1.8}_{+1.4}$	$^{+0.0}_{+0.1}$	$^{-0.1}_{+0.1}$	$^{+0.1}_{-0.1}$

Table 1: Continuation 2.

Q^2 (GeV^2)	x	N	$d^2\sigma/dxdQ^2$ (pb/GeV^2)	$\delta_{\rm stat}$ (%)	$\delta_{\rm sys}$ (%)	$\delta_{\rm u}$ (%)	δ_1 (%)	δ_2 (%)	δ_3 (%)	δ_4 (%)
3000	0.10	104	$9.11e-02$	$^{+9.8}_{-9.8}$	$^{+3.2}_{-3.0}$	$^{+2.9}_{-2.8}$	$^{-0.8}_{+0.6}$	$^{-0.7}_{+0.4}$	$^{+0.4}_{-0.4}$	$^{+0.0}_{-0.0}$
3000	0.12	106	$6.44e-02$	$^{+9.7}_{-9.7}$	$^{+2.9}_{-2.8}$	$^{+2.7}_{-2.7}$	$^{-0.6}_{+0.8}$	$^{-0.0}_{+0.2}$	$^{-0.0}_{+0.0}$	$^{+0.0}_{-0.0}$
3000	0.16	77	$4.65e-02$	$^{+11.4}_{-11.4}$	$^{+3.4}_{-3.4}$	$^{+3.4}_{-3.2}$	$^{-0.9}_{+0.7}$	$^{-0.1}_{+0.2}$	$^{-0.3}_{+0.3}$	$^{+0.0}_{-0.0}$
3000	0.19	82	$3.81e-02$	$^{+11.0}_{-11.0}$	$^{+3.4}_{-3.9}$	$^{+3.1}_{-3.2}$	$^{-1.4}_{+1.2}$	$^{-0.2}_{+0.1}$	$^{+0.5}_{-0.5}$	$^{+0.0}_{-0.0}$
3000	0.23	68	$3.15e-02$	$^{+12.1}_{-12.1}$	$^{+4.1}_{-3.8}$	$^{+3.8}_{-3.8}$	$^{+0.1}_{+0.6}$	$^{-0.4}_{+0.3}$	$^{-1.0}_{+1.0}$	$^{+0.0}_{-0.0}$
3000	0.28	58	$2.30e-02$	$^{+13.1}_{-13.1}$	$^{+4.4}_{-4.8}$	$^{+3.9}_{-3.9}$	$^{-1.8}_{+0.4}$	$^{-0.0}_{+0.2}$	$^{+1.9}_{-1.9}$	$^{+0.0}_{-0.0}$
3000	0.33	65	$2.10e-02$	$^{+12.4}_{-12.4}$	$^{+4.4}_{-4.5}$	$^{+4.3}_{-4.4}$	$^{-1.2}_{+0.6}$	$^{-0.0}_{-0.0}$	$^{-0.0}_{+0.0}$	$^{+0.0}_{-0.0}$
3000	0.39	26	$8.02e-03$	$^{+19.6}_{-19.6}$	$^{+6.5}_{-5.6}$	$^{+5.6}_{-5.3}$	$^{-1.4}_{+3.2}$	$^{-0.1}_{+0.0}$	$^{-1.1}_{+1.1}$	$^{+0.0}_{-0.0}$
3000	0.48	32	$5.33e-03$	$^{+17.7}_{-17.7}$	$^{+6.0}_{-5.7}$	$^{+5.6}_{-5.6}$	$^{-1.3}_{+2.2}$	$^{-0.2}_{+0.2}$	$^{-0.0}_{+0.0}$	$^{+0.1}_{-0.1}$
3500	0.12	151	$6.40e-02$	$^{+8.1}_{-8.1}$	$^{+2.7}_{-3.2}$	$^{+2.5}_{-2.5}$	$^{-1.5}_{+0.4}$	$^{-0.2}_{+0.2}$	$^{-0.7}_{+0.7}$	$^{+0.0}_{-0.0}$
3500	0.14	117	$4.68e-02$	$^{+9.2}_{-9.2}$	$^{+3.3}_{-3.1}$	$^{+2.8}_{-2.9}$	$^{-0.9}_{+1.5}$	$^{-0.3}_{+0.3}$	$^{+0.1}_{-0.1}$	$^{+0.0}_{-0.0}$
3500	0.18	90	$2.74e-02$	$^{+10.5}_{-10.5}$	$^{+3.2}_{-2.9}$	$^{+2.9}_{-2.9}$	$^{+0.2}_{+0.7}$	$^{-0.2}_{+0.3}$	$^{+0.6}_{-0.6}$	$^{+0.0}_{-0.0}$
3500	0.22	84	$2.56e-02$	$^{+10.9}_{-10.9}$	$^{+3.8}_{-3.9}$	$^{+3.4}_{-3.4}$	$^{-1.3}_{+0.8}$	$^{+0.0}_{-0.1}$	$^{-1.3}_{+1.3}$	$^{+0.0}_{-0.0}$
3500	0.26	76	$1.91e-02$	$^{+11.5}_{-11.5}$	$^{+4.1}_{-3.9}$	$^{+3.6}_{-3.6}$	$^{-0.9}_{+1.7}$	$^{-0.2}_{+0.3}$	$^{-0.1}_{+0.1}$	$^{+0.0}_{-0.0}$
3500	0.31	48	$1.22e-02$	$^{+14.4}_{-14.4}$	$^{+4.6}_{-4.5}$	$^{+4.3}_{-4.3}$	$^{-1.3}_{+1.3}$	$^{-0.2}_{+0.1}$	$^{+0.8}_{-0.8}$	$^{+0.0}_{-0.0}$
3500	0.37	34	$7.29e-03$	$^{+17.1}_{-17.1}$	$^{+5.9}_{-5.1}$	$^{+5.9}_{-4.7}$	$^{-1.3}_{+1.2}$	$^{-0.2}_{+0.2}$	$^{+1.2}_{-1.2}$	$^{+0.0}_{-0.0}$
3500	0.43	23	$5.02e-03$	$^{+20.9}_{-20.9}$	$^{+6.6}_{-7.2}$	$^{+6.0}_{-6.1}$	$^{-3.3}_{+2.5}$	$^{+0.1}_{-0.0}$	$^{-0.5}_{+0.5}$	$^{+0.1}_{-0.1}$
3500	0.52	33	$3.45e-03$	$^{+17.4}_{-17.4}$	$^{+6.7}_{-6.9}$	$^{+6.1}_{-6.1}$	$^{-1.6}_{+1.2}$	$^{-0.1}_{+0.1}$	$^{+2.4}_{-2.4}$	$^{+0.1}_{-0.1}$
4150	0.11	90	$4.25e-02$	$^{+10.5}_{-10.5}$	$^{+3.5}_{-3.7}$	$^{+3.1}_{-3.1}$	$^{-0.5}_{+1.4}$	$^{-0.5}_{-0.0}$	$^{-0.3}_{+0.3}$	$^{+0.0}_{-0.0}$
4150	0.14	98	$3.58e-02$	$^{+10.1}_{-10.1}$	$^{+3.5}_{-4.6}$	$^{+3.4}_{-3.4}$	$^{-1.5}_{+0.5}$	$^{-0.7}_{+0.7}$	$^{-0.3}_{+0.3}$	$^{+0.0}_{-0.0}$
4150	0.17	103	$2.72e-02$	$^{+9.9}_{-9.9}$	$^{+3.4}_{-3.5}$	$^{+3.0}_{-3.1}$	$^{-1.2}_{+1.3}$	$^{-0.2}_{+0.0}$	$^{-0.2}_{+0.2}$	$^{+0.0}_{-0.0}$
4150	0.21	69	$1.82e-02$	$^{+12.0}_{-12.0}$	$^{+4.2}_{-4.2}$	$^{+3.7}_{-3.7}$	$^{-1.7}_{+1.6}$	$^{-0.3}_{+0.3}$	$^{+1.2}_{-1.2}$	$^{+0.0}_{-0.0}$
4150	0.25	60	$1.31e-02$	$^{+12.9}_{-12.9}$	$^{+4.2}_{-4.4}$	$^{+3.8}_{-3.8}$	$^{-1.6}_{+0.9}$	$^{-0.1}_{+0.0}$	$^{+1.3}_{-1.3}$	$^{+0.0}_{-0.0}$
4150	0.31	47	$1.04e-02$	$^{+14.6}_{-14.6}$	$^{+4.7}_{-5.3}$	$^{+4.6}_{-4.6}$	$^{-1.8}_{+0.6}$	$^{-0.3}_{+0.2}$	$^{-1.1}_{+1.1}$	$^{+0.0}_{-0.0}$
4150	0.36	31	$6.02e-03$	$^{+18.0}_{-18.0}$	$^{+6.5}_{-6.2}$	$^{+6.9}_{-5.4}$	$^{-1.9}_{+1.0}$	$^{-0.0}_{+0.3}$	$^{+2.0}_{-2.0}$	$^{+0.0}_{-0.0}$
4150	0.42	24	$4.50e-03$	$^{+20.4}_{-20.4}$	$^{+7.6}_{-6.9}$	$^{+6.7}_{-6.4}$	$^{-2.6}_{+3.1}$	$^{-0.2}_{+0.3}$	$^{-0.5}_{+0.5}$	$^{+0.0}_{-0.0}$
4150	0.48	14	$2.62e-03$	$^{+30.3}_{-23.2}$	$^{+8.8}_{-10.1}$	$^{+8.3}_{-8.5}$	$^{-3.8}_{-0.1}$	$^{-0.1}_{-0.0}$	$^{-2.9}_{+2.9}$	$^{+0.1}_{-0.1}$
4150	0.57	18	$1.61e-03$	$^{+26.3}_{-20.8}$	$^{+9.8}_{-8.8}$	$^{+8.7}_{-8.7}$	$^{-1.4}_{+4.1}$	$^{+0.1}_{+0.1}$	$^{+0.7}_{-0.7}$	$^{+0.3}_{-0.3}$

Table 1: Continuation 3.

Q^2 (GeV^2)	x	N	$d^2\sigma/dxdQ^2$ ($\mathrm{pb/GeV}^2$)	δ_{stat} (%)	δ_{sys} (%)	δ_{u} (%)	δ_1 (%)	δ_2 (%)	δ_3 (%)	δ_4 (%)
5250	0.11	114	$2.59e-02$	$^{+9.4}_{-9.4}$	$^{+3.4}_{-3.2}$	$^{+2.9}_{-2.9}$	$^{-0.6}_{+1.1}$	$^{-0.0}_{+0.1}$	$^{-1.3}_{+1.3}$	$^{+0.0}_{-0.0}$
5250	0.14	117	$2.12e-02$	$^{+9.2}_{-9.2}$	$^{+3.6}_{-3.4}$	$^{+3.1}_{-2.7}$	$^{-1.8}_{+1.6}$	$^{-0.6}_{+0.6}$	$^{+0.4}_{-0.4}$	$^{+0.0}_{-0.0}$
5250	0.17	117	$2.06e-02$	$^{+9.2}_{-9.2}$	$^{+3.2}_{-3.4}$	$^{+3.1}_{-3.1}$	$^{-1.2}_{+0.5}$	$^{-0.5}_{+0.3}$	$^{+0.2}_{-0.2}$	$^{+0.0}_{-0.0}$
5250	0.20	91	$1.11e-02$	$^{+10.5}_{-10.5}$	$^{+3.3}_{-3.1}$	$^{+3.1}_{-2.9}$	$^{-0.5}_{+1.0}$	$^{+0.0}_{+0.2}$	$^{-0.7}_{+0.7}$	$^{+0.0}_{-0.0}$
5250	0.25	92	$9.27e-03$	$^{+10.4}_{-10.4}$	$^{+3.6}_{-4.2}$	$^{+3.1}_{-3.2}$	$^{-1.1}_{+1.5}$	$^{-0.4}_{+0.1}$	$^{+0.4}_{-0.4}$	$^{+0.0}_{-0.0}$
5250	0.29	52	$5.19e-03$	$^{+13.9}_{-13.9}$	$^{+4.4}_{-3.9}$	$^{+3.7}_{-3.7}$	$^{-0.2}_{+1.6}$	$^{-0.3}_{+0.3}$	$^{-1.0}_{+1.0}$	$^{+0.0}_{-0.0}$
5250	0.35	42	$3.66e-03$	$^{+15.4}_{-15.4}$	$^{+4.9}_{-5.3}$	$^{+4.2}_{-4.3}$	$^{-2.4}_{+2.3}$	$^{-0.3}_{+0.4}$	$^{+0.2}_{-0.2}$	$^{+0.0}_{-0.0}$
5250	0.41	14	$1.27e-03$	$^{+30.3}_{-23.2}$	$^{+6.0}_{-14.7}$	$^{+5.4}_{-5.5}$	$^{-1.9}_{+2.4}$	$^{-0.2}_{+0.0}$	$^{-0.3}_{+0.3}$	$^{+0.0}_{-0.0}$
5250	0.47	21	$1.83e-03$	$^{+21.8}_{-21.8}$	$^{+6.8}_{-7.1}$	$^{+6.7}_{-7.0}$	$^{-1.3}_{-0.3}$	$^{-0.1}_{+0.3}$	$^{+0.4}_{-0.4}$	$^{+0.1}_{-0.1}$
5250	0.53	14	$1.14e-03$	$^{+30.3}_{-23.2}$	$^{+9.1}_{-10.9}$	$^{+8.6}_{-8.6}$	$^{-2.3}_{+2.6}$	$^{+0.0}_{+0.0}$	$^{+0.6}_{-0.6}$	$^{+0.1}_{-0.1}$
5250	0.62	5	$1.76e-04$	$^{+55.2}_{-35.2}$	$^{+11.1}_{-10.5}$	$^{+9.2}_{-9.1}$	$^{-3.2}_{+4.6}$	$^{+0.1}_{+0.1}$	$^{+3.7}_{-3.7}$	$^{+0.6}_{-0.6}$
7000	0.12	93	$1.61e-02$	$^{+10.4}_{-10.4}$	$^{+4.0}_{-5.1}$	$^{+3.3}_{-3.6}$	$^{-1.1}_{+0.8}$	$^{+0.8}_{-0.5}$	$^{-0.7}_{+0.7}$	$^{+0.0}_{-0.0}$
7000	0.14	89	$1.25e-02$	$^{+10.6}_{-10.6}$	$^{+3.7}_{-5.2}$	$^{+3.4}_{-3.5}$	$^{-1.3}_{+1.2}$	$^{-0.5}_{+0.2}$	$^{-0.9}_{+0.9}$	$^{+0.0}_{-0.0}$
7000	0.18	68	$7.02e-03$	$^{+12.1}_{-12.1}$	$^{+3.9}_{-3.6}$	$^{+3.4}_{-3.4}$	$^{-0.6}_{+0.6}$	$^{-0.6}_{+0.4}$	$^{-0.4}_{+0.4}$	$^{+0.0}_{-0.0}$
7000	0.22	56	$5.60e-03$	$^{+13.4}_{-13.4}$	$^{+4.2}_{-4.2}$	$^{+3.9}_{-3.9}$	$^{-1.4}_{+1.1}$	$^{-0.4}_{+1.0}$	$^{-0.4}_{+0.4}$	$^{+0.0}_{-0.0}$
7000	0.26	49	$3.79e-03$	$^{+14.3}_{-14.3}$	$^{+4.6}_{-4.8}$	$^{+3.9}_{-4.0}$	$^{-0.2}_{+2.1}$	$^{+0.2}_{-0.2}$	$^{-0.5}_{+0.5}$	$^{+0.0}_{-0.0}$
7000	0.32	41	$2.70e-03$	$^{+15.6}_{-15.6}$	$^{+5.1}_{-4.7}$	$^{+5.3}_{-4.5}$	$^{-1.4}_{+0.8}$	$^{-0.4}_{+0.4}$	$^{-0.2}_{+0.2}$	$^{+0.0}_{-0.0}$
7000	0.38	23	$1.52e-03$	$^{+20.9}_{-20.9}$	$^{+6.4}_{-6.2}$	$^{+5.5}_{-5.5}$	$^{-1.8}_{+1.7}$	$^{-0.7}_{+0.4}$	$^{+2.0}_{-2.0}$	$^{+0.0}_{-0.0}$
7000	0.44	17	$1.15e-03$	$^{+27.2}_{-21.3}$	$^{+8.4}_{-7.9}$	$^{+7.1}_{-7.1}$	$^{-2.7}_{+2.7}$	$^{-0.0}_{+0.2}$	$^{-2.4}_{+2.4}$	$^{+0.0}_{-0.0}$
7000	0.50	8	$5.38e-04$	$^{+41.8}_{-29.4}$	$^{+9.7}_{-10.3}$	$^{+9.5}_{-9.5}$	$^{-1.6}_{+1.4}$	$^{-0.3}_{+0.4}$	$^{+2.4}_{-2.4}$	$^{+0.1}_{-0.1}$
7000	0.56	4	$2.37e-04$	$^{+63.2}_{-38.2}$	$^{+12.3}_{-11.8}$	$^{+11.3}_{-11.3}$	$^{-3.4}_{+3.4}$	$^{+0.1}_{-0.0}$	$^{+1.2}_{-1.2}$	$^{+0.2}_{-0.2}$
7000	0.66	10	$2.30e-04$	$^{+36.7}_{-26.8}$	$^{+12.6}_{-13.6}$	$^{+12.1}_{-12.3}$	$^{-4.3}_{+2.5}$	$^{-0.3}_{-0.0}$	$^{+2.0}_{-2.0}$	$^{+0.9}_{-0.9}$
9500	0.17	76	$6.77e-03$	$^{+11.5}_{-11.5}$	$^{+5.6}_{-7.7}$	$^{+4.9}_{-4.9}$	$^{-2.0}_{+2.3}$	$^{+0.2}_{-0.2}$	$^{-0.6}_{+0.6}$	$^{+0.0}_{-0.0}$
9500	0.21	53	$3.87e-03$	$^{+13.7}_{-13.7}$	$^{+5.8}_{-5.1}$	$^{+4.3}_{-4.5}$	$^{-1.1}_{+1.8}$	$^{-0.7}_{+0.4}$	$^{-1.1}_{+1.1}$	$^{+0.0}_{-0.0}$
9500	0.25	40	$2.27e-03$	$^{+15.8}_{-15.8}$	$^{+4.8}_{-4.9}$	$^{+4.5}_{-4.5}$	$^{-2.0}_{+1.5}$	$^{+0.2}_{+0.4}$	$^{+0.1}_{-0.1}$	$^{+0.0}_{-0.0}$
9500	0.31	27	$1.50e-03$	$^{+19.2}_{-19.2}$	$^{+5.7}_{-8.1}$	$^{+5.2}_{-5.3}$	$^{-2.6}_{+1.5}$	$^{-0.5}_{+0.2}$	$^{+1.5}_{-1.5}$	$^{+0.0}_{-0.0}$
9500	0.36	19	$8.89e-04$	$^{+25.5}_{-20.3}$	$^{+6.6}_{-6.1}$	$^{+5.9}_{-5.9}$	$^{-1.0}_{+1.9}$	$^{-0.4}_{+0.2}$	$^{-0.3}_{+0.3}$	$^{+0.0}_{-0.0}$
9500	0.42	12	$5.64e-04$	$^{+33.1}_{-24.8}$	$^{+11.3}_{-7.5}$	$^{+13.4}_{-7.3}$	$^{-1.0}_{+2.4}$	$^{-0.8}_{+0.5}$	$^{-0.8}_{+0.8}$	$^{+0.0}_{-0.0}$
9500	0.48	8	$3.63e-04$	$^{+41.7}_{-29.4}$	$^{+10.5}_{-10.4}$	$^{+9.2}_{-9.2}$	$^{-2.6}_{+2.4}$	$^{-0.4}_{+0.6}$	$^{-3.4}_{+3.4}$	$^{+0.0}_{-0.0}$
9500	0.54	5	$2.31e-04$	$^{+55.2}_{-35.2}$	$^{+14.3}_{-13.7}$	$^{+12.5}_{-12.2}$	$^{-1.7}_{+3.6}$	$^{-0.2}_{+0.6}$	$^{+5.7}_{-5.7}$	$^{+0.1}_{-0.1}$
9500	0.61	4	$1.39e-04$	$^{+63.3}_{-38.3}$	$^{+15.5}_{-15.4}$	$^{+14.6}_{-14.8}$	$^{-4.2}_{+4.2}$	$^{+0.0}_{-0.1}$	$^{+0.4}_{-0.4}$	$^{+0.4}_{-0.4}$
9500	0.71	1	$1.50e-05$	$^{+158.0}_{-58.0}$	$^{+21.1}_{-19.8}$	$^{+18.9}_{-18.9}$	$^{-3.3}_{+4.5}$	$^{-0.4}_{+0.3}$	$^{+4.8}_{-4.8}$	$^{+1.3}_{-1.3}$

Table 1: Continuation 4.

Q^2 (GeV^2)	x	N	$d^2\sigma/dxdQ^2$ ($\mathrm{pb/GeV}^2$)	δ_{stat} (%)	δ_{sys} (%)	δ_{u} (%)	δ_1 (%)	δ_2 (%)	δ_3 (%)	δ_4 (%)
15500	0.43	120	$3.22e-04$	$^{+9.1}_{-9.1}$	$^{+5.5}_{-5.1}$	$^{+3.0}_{-3.0}$	$^{-2.8}_{+3.0}$	$^{-0.8}_{+0.7}$	$^{-0.7}_{+0.7}$	$^{+0.1}_{-0.1}$
15500	0.80	8	$3.39e-06$	$^{+41.8}_{-29.4}$	$^{+15.3}_{-14.9}$	$^{+12.9}_{-12.9}$	$^{-5.3}_{+4.7}$	$^{+0.0}_{+0.4}$	$^{+3.2}_{-3.2}$	$^{+3.0}_{-3.0}$

Table 1: Continuation 5.

Q^2 (GeV^2)	x	N	$d^2\sigma/dxdQ^2$ (pb/GeV^2)	$\delta_{\rm stat}$ (%)	$\delta_{\rm sys}$ (%)	$\delta_{\rm u}$ (%)	δ_1 (%)	δ_2 (%)	δ_3 (%)	δ_4 (%)
725	0.06	567	$3.31e+00$	$^{+4.2}_{-4.2}$	$^{+1.6}_{-1.8}$	$^{+1.3}_{-1.3}$	$^{+0.8}_{-1.0}$	$^{+0.0}_{+0.0}$	$^{-0.1}_{+0.1}$	$^{+0.1}_{-0.1}$
725	0.08	418	$2.42e+00$	$^{+4.9}_{-4.9}$	$^{+1.9}_{-2.0}$	$^{+1.5}_{-1.4}$	$^{+1.1}_{-0.9}$	$^{-0.2}_{+0.0}$	$^{-0.3}_{+0.3}$	$^{+0.1}_{-0.1}$
725	0.10	321	$1.81e+00$	$^{+5.6}_{-5.6}$	$^{+2.0}_{-2.1}$	$^{+1.7}_{-1.7}$	$^{+0.9}_{-1.2}$	$^{-0.0}_{+0.4}$	$^{-0.1}_{+0.1}$	$^{+0.1}_{-0.1}$
725	0.12	274	$1.27e+00$	$^{+6.0}_{-6.0}$	$^{+2.5}_{-2.8}$	$^{+2.1}_{-1.8}$	$^{+1.4}_{-1.8}$	$^{-0.1}_{-0.1}$	$^{-0.1}_{+0.1}$	$^{+0.1}_{-0.1}$
725	0.16	207	$1.04e+00$	$^{+7.0}_{-7.0}$	$^{+3.9}_{-3.2}$	$^{+2.4}_{-2.1}$	$^{+1.8}_{-1.4}$	$^{-0.1}_{+0.2}$	$^{+1.9}_{-1.9}$	$^{+0.1}_{-0.1}$
725	0.19	176	$7.00e-01$	$^{+7.5}_{-7.5}$	$^{+2.9}_{-2.7}$	$^{+2.2}_{-2.4}$	$^{+1.4}_{-1.3}$	$^{-0.1}_{-0.0}$	$^{+0.6}_{-0.6}$	$^{+0.1}_{-0.1}$
725	0.23	152	$5.22e-01$	$^{+8.1}_{-8.1}$	$^{+3.1}_{-3.1}$	$^{+2.7}_{-2.4}$	$^{+1.6}_{-1.6}$	$^{+0.1}_{-0.0}$	$^{-0.5}_{+0.5}$	$^{+0.1}_{-0.1}$
875	0.05	599	$2.99e+00$	$^{+4.1}_{-4.1}$	$^{+1.5}_{-1.9}$	$^{+1.3}_{-1.4}$	$^{-1.1}_{+0.1}$	$^{-0.1}_{+0.3}$	$^{+0.2}_{-0.2}$	$^{+0.1}_{-0.1}$
875	0.07	497	$2.01e+00$	$^{+4.5}_{-4.5}$	$^{+2.3}_{-1.7}$	$^{+1.4}_{-1.4}$	$^{-0.6}_{+1.3}$	$^{-0.1}_{-0.2}$	$^{+0.0}_{-0.0}$	$^{+0.1}_{-0.1}$
875	0.09	407	$1.41e+00$	$^{+5.0}_{-5.0}$	$^{+2.0}_{-1.9}$	$^{+1.4}_{-1.4}$	$^{-0.6}_{+0.5}$	$^{+0.1}_{+0.2}$	$^{-1.0}_{+1.0}$	$^{+0.1}_{-0.1}$
875	0.11	351	$1.13e+00$	$^{+5.3}_{-5.3}$	$^{+1.8}_{-1.8}$	$^{+1.6}_{-1.6}$	$^{-0.4}_{+0.3}$	$^{-0.3}_{+0.0}$	$^{+0.4}_{-0.4}$	$^{+0.1}_{-0.1}$
875	0.14	288	$7.88e-01$	$^{+5.9}_{-5.9}$	$^{+2.1}_{-2.1}$	$^{+1.7}_{-1.7}$	$^{-0.5}_{+0.1}$	$^{-0.2}_{+0.1}$	$^{+1.1}_{-1.1}$	$^{+0.1}_{-0.1}$
875	0.17	291	$6.05e-01$	$^{+5.9}_{-5.9}$	$^{+1.8}_{-1.9}$	$^{+1.8}_{-1.8}$	$^{+0.2}_{-0.6}$	$^{-0.1}_{+0.3}$	$^{-0.0}_{+0.0}$	$^{+0.1}_{-0.1}$
875	0.21	199	$4.18e-01$	$^{+7.1}_{-7.1}$	$^{+2.3}_{-2.1}$	$^{+2.1}_{-2.2}$	$^{+0.4}_{+0.2}$	$^{+0.1}_{-0.1}$	$^{+0.0}_{-0.0}$	$^{+0.0}_{-0.0}$
875	0.25	185	$3.24e-01$	$^{+7.4}_{-7.4}$	$^{+2.3}_{-2.5}$	$^{+2.2}_{-2.3}$	$^{+0.2}_{-0.1}$	$^{+0.1}_{-0.0}$	$^{-0.5}_{+0.5}$	$^{+0.0}_{-0.0}$
1025	0.05	433	$2.11e+00$	$^{+4.8}_{-4.8}$	$^{+2.3}_{-1.9}$	$^{+1.6}_{-1.6}$	$^{-0.5}_{+1.1}$	$^{-0.0}_{+0.4}$	$^{+0.2}_{-0.2}$	$^{+0.1}_{-0.1}$
1025	0.07	344	$1.37e+00$	$^{+5.4}_{-5.4}$	$^{+1.7}_{-1.7}$	$^{+1.5}_{-1.6}$	$^{+0.1}_{+0.3}$	$^{-0.1}_{-0.0}$	$^{-0.6}_{+0.6}$	$^{+0.1}_{-0.1}$
1025	0.09	314	$1.03e+00$	$^{+5.6}_{-5.6}$	$^{+1.8}_{-2.4}$	$^{+1.6}_{-1.7}$	$^{-1.2}_{+0.2}$	$^{+0.1}_{+0.0}$	$^{+0.1}_{-0.1}$	$^{+0.1}_{-0.1}$
1025	0.11	275	$7.78e-01$	$^{+6.0}_{-6.0}$	$^{+2.2}_{-2.0}$	$^{+1.8}_{-1.8}$	$^{+0.0}_{+1.0}$	$^{-0.1}_{+0.3}$	$^{-0.6}_{+0.6}$	$^{+0.1}_{-0.1}$
1025	0.14	255	$6.03e-01$	$^{+6.3}_{-6.3}$	$^{+3.4}_{-2.1}$	$^{+1.9}_{-1.9}$	$^{-0.6}_{+1.7}$	$^{-0.1}_{-0.1}$	$^{+0.0}_{-0.0}$	$^{+0.1}_{-0.1}$
1025	0.17	184	$4.69e-01$	$^{+7.4}_{-7.4}$	$^{+3.0}_{-3.3}$	$^{+2.3}_{-2.5}$	$^{-1.3}_{+1.2}$	$^{-0.3}_{+0.2}$	$^{+1.0}_{-1.0}$	$^{+0.1}_{-0.1}$
1025	0.20	190	$3.64e-01$	$^{+7.3}_{-7.3}$	$^{+3.2}_{-2.8}$	$^{+2.8}_{-2.2}$	$^{-0.9}_{+0.9}$	$^{-0.2}_{+0.3}$	$^{-1.0}_{+1.0}$	$^{+0.0}_{-0.0}$
1025	0.27	284	$2.16e-01$	$^{+5.9}_{-5.9}$	$^{+3.3}_{-2.8}$	$^{+1.9}_{-1.8}$	$^{-1.6}_{+2.2}$	$^{+0.1}_{+0.0}$	$^{-0.2}_{+0.2}$	$^{+0.0}_{-0.0}$

Table 2: The double-differential cross section, $d^2\sigma/dxdQ^2$, for NC e^+p scattering at $\sqrt{s} = 318\,\text{GeV}$ as a function of Q^2 and x. Also quoted are the number of events reconstructed and selected in the bin, N, the statistical uncertainty, $\delta_{\rm stat}$, the total systematic uncertainty, $\delta_{\rm sys}$, the total uncorrelated systematic uncertainty, $\delta_{\rm u}$, followed by the bin-to-bin correlated systematic uncertainties, δ_1–δ_4, defined in Section 9. The upper limit on the cross section is given if no event is observed. The luminosity uncertainty of 1.8% is not included. This table has five continuations.

Q^2 (GeV^2)	x	N	$d^2\sigma/dxdQ^2$ (pb/GeV^2)	$\delta_{\rm stat}$ (%)	$\delta_{\rm sys}$ (%)	$\delta_{\rm u}$ (%)	δ_1 (%)	δ_2 (%)	δ_3 (%)	δ_4 (%)
1200	0.06	377	$1.35e+00$	$^{+5.2}_{-5.2}$	$^{+2.1}_{-2.3}$	$^{+1.7}_{-1.7}$	$^{-1.0}_{+0.9}$	$^{-0.5}_{+0.5}$	$^{-0.5}_{+0.5}$	$^{+0.1}_{-0.1}$
1200	0.07	314	$9.50e-01$	$^{+5.6}_{-5.6}$	$^{+1.9}_{-2.5}$	$^{+1.7}_{-1.7}$	$^{-1.2}_{+0.2}$	$^{-0.0}_{-0.0}$	$^{+0.7}_{-0.7}$	$^{+0.1}_{-0.1}$
1200	0.09	285	$6.97e-01$	$^{+5.9}_{-5.9}$	$^{+1.9}_{-2.1}$	$^{+1.7}_{-1.7}$	$^{-0.8}_{+0.4}$	$^{-0.2}_{+0.2}$	$^{-0.2}_{+0.2}$	$^{+0.1}_{-0.1}$
1200	0.12	325	$5.33e-01$	$^{+5.5}_{-5.5}$	$^{+2.7}_{-2.2}$	$^{+1.9}_{-1.8}$	$^{-1.2}_{+1.2}$	$^{+0.3}_{+0.0}$	$^{-0.6}_{+0.6}$	$^{+0.1}_{-0.1}$
1200	0.14	213	$3.76e-01$	$^{+6.9}_{-6.9}$	$^{+2.2}_{-3.3}$	$^{+2.0}_{-2.1}$	$^{-0.5}_{-0.4}$	$^{-0.5}_{+0.3}$	$^{-0.9}_{+0.9}$	$^{+0.1}_{-0.1}$
1200	0.18	210	$2.94e-01$	$^{+6.9}_{-6.9}$	$^{+2.8}_{-3.2}$	$^{+2.1}_{-2.4}$	$^{-0.8}_{-0.0}$	$^{-0.2}_{+0.0}$	$^{+1.8}_{-1.8}$	$^{+0.0}_{-0.0}$
1200	0.22	143	$1.95e-01$	$^{+8.4}_{-8.4}$	$^{+3.0}_{-2.7}$	$^{+2.6}_{-2.4}$	$^{-0.6}_{+0.7}$	$^{-0.0}_{+0.1}$	$^{-1.2}_{+1.2}$	$^{+0.0}_{-0.0}$
1200	0.29	219	$1.23e-01$	$^{+6.8}_{-6.8}$	$^{+2.5}_{-2.7}$	$^{+2.0}_{-2.0}$	$^{-1.3}_{+1.2}$	$^{-0.0}_{-0.1}$	$^{-0.5}_{+0.5}$	$^{+0.0}_{-0.0}$
1400	0.06	262	$8.59e-01$	$^{+6.2}_{-6.2}$	$^{+2.4}_{-2.3}$	$^{+2.0}_{-1.9}$	$^{-0.7}_{+0.9}$	$^{-0.2}_{+0.2}$	$^{-0.8}_{+0.8}$	$^{+0.1}_{-0.1}$
1400	0.08	230	$6.34e-01$	$^{+6.6}_{-6.6}$	$^{+2.6}_{-2.3}$	$^{+2.0}_{-2.0}$	$^{-0.8}_{+1.4}$	$^{-0.3}_{+0.1}$	$^{+0.2}_{-0.2}$	$^{+0.1}_{-0.1}$
1400	0.10	206	$4.53e-01$	$^{+7.0}_{-7.0}$	$^{+2.7}_{-2.5}$	$^{+2.0}_{-2.0}$	$^{-1.0}_{+1.2}$	$^{-0.0}_{+0.2}$	$^{-0.6}_{+0.6}$	$^{+0.1}_{-0.1}$
1400	0.12	197	$3.25e-01$	$^{+7.1}_{-7.1}$	$^{+2.3}_{-2.2}$	$^{+2.0}_{-2.0}$	$^{-0.6}_{+0.8}$	$^{-0.1}_{+0.2}$	$^{+0.1}_{-0.1}$	$^{+0.1}_{-0.1}$
1400	0.16	153	$2.63e-01$	$^{+8.1}_{-8.1}$	$^{+3.2}_{-2.6}$	$^{+2.4}_{-2.4}$	$^{-0.8}_{+1.5}$	$^{-0.2}_{+0.2}$	$^{-0.3}_{+0.3}$	$^{+0.0}_{-0.0}$
1400	0.19	148	$1.99e-01$	$^{+8.2}_{-8.2}$	$^{+2.5}_{-2.9}$	$^{+2.5}_{-2.6}$	$^{-0.6}_{+0.2}$	$^{-0.1}_{+0.1}$	$^{+0.2}_{-0.2}$	$^{+0.0}_{-0.0}$
1400	0.23	107	$1.42e-01$	$^{+9.7}_{-9.7}$	$^{+3.6}_{-3.1}$	$^{+3.0}_{-2.9}$	$^{-0.9}_{+1.4}$	$^{-0.2}_{+0.1}$	$^{-0.1}_{+0.1}$	$^{+0.0}_{-0.0}$
1400	0.31	180	$8.96e-02$	$^{+7.5}_{-7.5}$	$^{+2.8}_{-2.8}$	$^{+2.4}_{-2.3}$	$^{-0.9}_{+0.8}$	$^{+0.0}_{-0.0}$	$^{-1.0}_{+1.0}$	$^{+0.0}_{-0.0}$
1650	0.05	288	$6.76e-01$	$^{+5.9}_{-5.9}$	$^{+2.0}_{-2.5}$	$^{+1.9}_{-1.9}$	$^{-1.1}_{+0.5}$	$^{-0.3}_{+0.2}$	$^{+0.0}_{-0.0}$	$^{+0.0}_{-0.0}$
1650	0.07	281	$5.74e-01$	$^{+6.0}_{-6.0}$	$^{+2.3}_{-2.2}$	$^{+1.9}_{-1.9}$	$^{-0.4}_{+0.6}$	$^{-0.2}_{+0.2}$	$^{-0.9}_{+0.9}$	$^{+0.0}_{-0.0}$
1650	0.09	244	$4.04e-01$	$^{+6.4}_{-6.4}$	$^{+2.1}_{-2.3}$	$^{+1.9}_{-1.9}$	$^{-1.0}_{+0.6}$	$^{-0.1}_{+0.3}$	$^{-0.1}_{+0.1}$	$^{+0.1}_{-0.1}$
1650	0.11	223	$3.00e-01$	$^{+6.7}_{-6.7}$	$^{+2.1}_{-2.4}$	$^{+2.0}_{-2.0}$	$^{-1.0}_{+0.6}$	$^{-0.1}_{+0.0}$	$^{-0.5}_{+0.5}$	$^{+0.1}_{-0.1}$
1650	0.14	225	$2.42e-01$	$^{+6.7}_{-6.7}$	$^{+2.4}_{-2.5}$	$^{+2.1}_{-2.1}$	$^{-1.0}_{+0.7}$	$^{-0.1}_{+0.0}$	$^{-0.8}_{+0.8}$	$^{+0.0}_{-0.0}$
1650	0.17	202	$1.72e-01$	$^{+7.0}_{-7.0}$	$^{+2.6}_{-2.4}$	$^{+2.1}_{-2.1}$	$^{-0.6}_{+0.9}$	$^{-0.2}_{+0.2}$	$^{+0.9}_{-0.9}$	$^{+0.0}_{-0.0}$
1650	0.21	147	$1.29e-01$	$^{+8.2}_{-8.2}$	$^{+3.1}_{-2.7}$	$^{+2.5}_{-2.5}$	$^{-0.4}_{+1.4}$	$^{-0.2}_{+0.2}$	$^{+0.3}_{-0.3}$	$^{+0.0}_{-0.0}$
1650	0.25	119	$8.47e-02$	$^{+9.2}_{-9.2}$	$^{+2.9}_{-3.2}$	$^{+2.7}_{-2.8}$	$^{-1.3}_{+0.7}$	$^{-0.1}_{+0.1}$	$^{+0.3}_{-0.3}$	$^{+0.0}_{-0.0}$
1650	0.34	167	$5.49e-02$	$^{+7.7}_{-7.7}$	$^{+3.1}_{-2.9}$	$^{+2.4}_{-2.4}$	$^{-1.3}_{+1.5}$	$^{-0.0}_{+0.0}$	$^{-0.2}_{+0.2}$	$^{+0.0}_{-0.0}$

Table 2: Continuation 1.

Q^2 (GeV^2)	x	N	$d^2\sigma/dxdQ^2$ (pb/GeV^2)	$\delta_{\rm stat}$ (%)	$\delta_{\rm sys}$ (%)	$\delta_{\rm u}$ (%)	δ_1 (%)	δ_2 (%)	δ_3 (%)	δ_4 (%)
1950	0.06	180	$3.86e-01$	$^{+7.5}_{-7.5}$	$^{+2.9}_{-2.6}$	$^{+2.3}_{-2.3}$	$^{-1.0}_{+1.3}$	$^{-0.2}_{+0.1}$	$^{-0.6}_{+0.6}$	$^{+0.0}_{-0.0}$
1950	0.08	161	$3.07e-01$	$^{+7.9}_{-7.9}$	$^{+2.6}_{-2.7}$	$^{+2.3}_{-2.4}$	$^{-1.0}_{+0.8}$	$^{-0.4}_{+0.3}$	$^{-0.6}_{+0.6}$	$^{+0.0}_{-0.0}$
1950	0.10	161	$2.33e-01$	$^{+7.9}_{-7.9}$	$^{+2.8}_{-2.8}$	$^{+2.3}_{-2.4}$	$^{+0.0}_{+0.8}$	$^{-0.2}_{+0.3}$	$^{-1.1}_{+1.1}$	$^{+0.0}_{-0.0}$
1950	0.12	146	$1.55e-01$	$^{+8.3}_{-8.3}$	$^{+2.5}_{-2.6}$	$^{+2.4}_{-2.3}$	$^{-1.0}_{+0.6}$	$^{-0.2}_{+0.2}$	$^{-0.4}_{+0.4}$	$^{+0.0}_{-0.0}$
1950	0.16	117	$1.29e-01$	$^{+9.2}_{-9.2}$	$^{+3.1}_{-2.9}$	$^{+2.7}_{-2.7}$	$^{-0.9}_{+1.2}$	$^{-0.1}_{+0.1}$	$^{-0.3}_{+0.3}$	$^{+0.0}_{-0.0}$
1950	0.19	94	$7.79e-02$	$^{+10.3}_{-10.3}$	$^{+3.2}_{-3.1}$	$^{+2.7}_{-2.7}$	$^{-1.0}_{+1.1}$	$^{-0.2}_{+0.0}$	$^{-0.8}_{+0.8}$	$^{+0.0}_{-0.0}$
1950	0.23	79	$5.58e-02$	$^{+11.3}_{-11.3}$	$^{+3.1}_{-3.1}$	$^{+2.9}_{-2.9}$	$^{-0.8}_{+0.5}$	$^{-0.1}_{+0.1}$	$^{-0.4}_{+0.4}$	$^{+0.0}_{-0.0}$
1950	0.28	65	$4.50e-02$	$^{+12.4}_{-12.4}$	$^{+3.8}_{-3.8}$	$^{+3.5}_{-3.5}$	$^{-0.9}_{+1.0}$	$^{-0.1}_{+0.2}$	$^{-0.3}_{+0.3}$	$^{+0.0}_{-0.0}$
1950	0.37	85	$2.50e-02$	$^{+10.8}_{-10.8}$	$^{+3.6}_{-4.1}$	$^{+3.0}_{-3.1}$	$^{-1.5}_{+1.6}$	$^{-0.0}_{+0.0}$	$^{-0.7}_{+0.7}$	$^{+0.0}_{-0.0}$
2250	0.06	135	$3.22e-01$	$^{+8.6}_{-8.6}$	$^{+3.1}_{-3.2}$	$^{+2.7}_{-2.7}$	$^{-1.3}_{+1.0}$	$^{-0.2}_{+0.3}$	$^{+0.9}_{-0.9}$	$^{+0.0}_{-0.0}$
2250	0.07	122	$2.47e-01$	$^{+9.1}_{-9.1}$	$^{+3.2}_{-3.0}$	$^{+2.8}_{-2.8}$	$^{-0.8}_{+1.2}$	$^{-0.6}_{+0.6}$	$^{-0.4}_{+0.4}$	$^{+0.0}_{-0.0}$
2250	0.09	114	$1.93e-01$	$^{+9.4}_{-9.4}$	$^{+3.0}_{-3.1}$	$^{+2.8}_{-2.8}$	$^{-1.0}_{+0.8}$	$^{-0.3}_{-0.1}$	$^{-0.5}_{+0.5}$	$^{+0.0}_{-0.0}$
2250	0.12	134	$1.42e-01$	$^{+8.6}_{-8.6}$	$^{+2.9}_{-2.9}$	$^{+2.6}_{-2.6}$	$^{-1.0}_{+0.8}$	$^{-0.1}_{+0.4}$	$^{-0.1}_{+0.1}$	$^{+0.0}_{-0.0}$
2250	0.14	81	$8.71e-02$	$^{+11.1}_{-11.1}$	$^{+3.4}_{-3.2}$	$^{+3.1}_{-3.1}$	$^{-0.6}_{+1.1}$	$^{+0.0}_{+0.2}$	$^{-0.2}_{+0.2}$	$^{+0.0}_{-0.0}$
2250	0.18	83	$6.94e-02$	$^{+11.0}_{-11.0}$	$^{+3.4}_{-3.4}$	$^{+3.0}_{-3.1}$	$^{-1.0}_{+0.7}$	$^{-0.4}_{+0.2}$	$^{+1.1}_{-1.1}$	$^{+0.0}_{-0.0}$
2250	0.22	51	$4.36e-02$	$^{+14.0}_{-14.0}$	$^{+4.0}_{-3.8}$	$^{+3.6}_{-3.6}$	$^{-0.9}_{+1.6}$	$^{+0.1}_{+0.0}$	$^{-0.6}_{+0.6}$	$^{+0.0}_{-0.0}$
2250	0.26	66	$4.61e-02$	$^{+12.3}_{-12.3}$	$^{+4.1}_{-4.9}$	$^{+3.8}_{-3.9}$	$^{-1.5}_{+1.1}$	$^{-0.3}_{+0.2}$	$^{-1.1}_{+1.1}$	$^{+0.0}_{-0.0}$
2250	0.31	30	$2.04e-02$	$^{+18.3}_{-18.3}$	$^{+4.7}_{-4.5}$	$^{+4.6}_{-4.5}$	$^{-0.1}_{+0.6}$	$^{-0.2}_{+0.1}$	$^{-0.1}_{+0.1}$	$^{+0.0}_{-0.0}$
2250	0.40	53	$1.54e-02$	$^{+13.7}_{-13.7}$	$^{+4.8}_{-5.0}$	$^{+4.6}_{-3.9}$	$^{-2.5}_{+1.8}$	$^{+0.0}_{+0.0}$	$^{-0.6}_{+0.6}$	$^{+0.1}_{-0.1}$
2600	0.09	110	$1.40e-01$	$^{+9.5}_{-9.5}$	$^{+3.1}_{-2.9}$	$^{+2.8}_{-2.8}$	$^{-0.7}_{+1.2}$	$^{-0.1}_{+0.1}$	$^{-0.4}_{+0.4}$	$^{+0.0}_{-0.0}$
2600	0.11	111	$1.16e-01$	$^{+9.5}_{-9.5}$	$^{+2.9}_{-3.2}$	$^{+2.9}_{-2.9}$	$^{-1.2}_{+0.3}$	$^{-0.4}_{+0.2}$	$^{+0.5}_{-0.5}$	$^{+0.0}_{-0.0}$
2600	0.14	110	$8.85e-02$	$^{+9.5}_{-9.5}$	$^{+3.3}_{-3.3}$	$^{+2.9}_{-2.9}$	$^{-1.2}_{+1.4}$	$^{-0.0}_{+0.3}$	$^{+0.0}_{-0.0}$	$^{+0.0}_{-0.0}$
2600	0.17	87	$6.93e-02$	$^{+10.7}_{-10.7}$	$^{+3.5}_{-3.3}$	$^{+3.3}_{-3.3}$	$^{-0.1}_{+0.8}$	$^{-0.3}_{+0.3}$	$^{+0.2}_{-0.2}$	$^{+0.0}_{-0.0}$
2600	0.20	65	$4.00e-02$	$^{+12.4}_{-12.4}$	$^{+3.4}_{-3.5}$	$^{+3.3}_{-3.3}$	$^{-1.0}_{+0.4}$	$^{-0.1}_{+0.2}$	$^{-0.5}_{+0.5}$	$^{+0.0}_{-0.0}$
2600	0.25	71	$3.71e-02$	$^{+11.9}_{-11.9}$	$^{+4.0}_{-3.9}$	$^{+3.7}_{-3.7}$	$^{-1.0}_{+1.0}$	$^{-0.1}_{+0.0}$	$^{+0.7}_{-0.7}$	$^{+0.0}_{-0.0}$
2600	0.29	41	$2.13e-02$	$^{+15.6}_{-15.6}$	$^{+5.0}_{-5.2}$	$^{+4.2}_{-4.2}$	$^{-1.5}_{+0.6}$	$^{-0.1}_{+0.0}$	$^{-2.5}_{+2.5}$	$^{+0.0}_{-0.0}$
2600	0.35	36	$1.54e-02$	$^{+16.7}_{-16.7}$	$^{+5.3}_{-5.3}$	$^{+4.6}_{-4.6}$	$^{-0.6}_{+2.0}$	$^{-0.1}_{+0.4}$	$^{+0.2}_{-0.2}$	$^{+0.0}_{-0.0}$
2600	0.44	47	$1.03e-02$	$^{+14.6}_{-14.6}$	$^{+5.3}_{-5.5}$	$^{+4.6}_{-4.7}$	$^{-2.0}_{+1.0}$	$^{+0.0}_{-0.1}$	$^{-2.0}_{+2.0}$	$^{+0.1}_{-0.1}$

Table 2: Continuation 2.

Q^2 (GeV^2)	x	N	$d^2\sigma/dxdQ^2$ (pb/GeV^2)	$\delta_{\rm stat}$ (%)	$\delta_{\rm sys}$ (%)	$\delta_{\rm u}$ (%)	δ_1 (%)	δ_2 (%)	δ_3 (%)	δ_4 (%)
3000	0.10	75	$8.89e-02$	$^{+11.5}_{-11.5}$	$^{+3.7}_{-3.5}$	$^{+3.5}_{-3.5}$	$^{-0.1}_{+0.9}$	$^{-0.5}_{+0.7}$	$^{+0.0}_{-0.0}$	$^{+0.0}_{-0.0}$
3000	0.12	99	$8.21e-02$	$^{+10.1}_{-10.1}$	$^{+3.4}_{-3.4}$	$^{+3.3}_{-3.3}$	$^{-1.0}_{+0.6}$	$^{-0.2}_{-0.0}$	$^{+0.3}_{-0.3}$	$^{+0.0}_{-0.0}$
3000	0.16	79	$6.51e-02$	$^{+11.3}_{-11.3}$	$^{+3.9}_{-4.4}$	$^{+3.7}_{-3.8}$	$^{-1.8}_{+0.9}$	$^{-0.1}_{+0.1}$	$^{+0.5}_{-0.5}$	$^{+0.0}_{-0.0}$
3000	0.19	61	$3.67e-02$	$^{+12.8}_{-12.8}$	$^{+3.8}_{-4.4}$	$^{+3.6}_{-3.7}$	$^{-0.1}_{+0.9}$	$^{-0.1}_{+0.1}$	$^{-0.0}_{+0.0}$	$^{+0.0}_{-0.0}$
3000	0.23	48	$3.03e-02$	$^{+14.4}_{-14.4}$	$^{+4.4}_{-5.1}$	$^{+4.3}_{-4.3}$	$^{-2.5}_{+0.4}$	$^{-0.3}_{+0.4}$	$^{+0.6}_{-0.6}$	$^{+0.0}_{-0.0}$
3000	0.28	46	$2.33e-02$	$^{+14.7}_{-14.7}$	$^{+5.0}_{-4.5}$	$^{+4.5}_{-4.5}$	$^{-0.2}_{+1.7}$	$^{-0.1}_{+0.3}$	$^{+0.0}_{-0.0}$	$^{+0.0}_{-0.0}$
3000	0.33	30	$1.26e-02$	$^{+18.3}_{-18.3}$	$^{+5.1}_{-5.5}$	$^{+5.0}_{-5.0}$	$^{-1.9}_{+1.0}$	$^{-0.3}_{+0.0}$	$^{-0.3}_{+0.3}$	$^{+0.0}_{-0.0}$
3000	0.39	13	$5.39e-03$	$^{+31.5}_{-23.9}$	$^{+6.7}_{-6.6}$	$^{+6.5}_{-6.1}$	$^{-1.8}_{+1.3}$	$^{+0.0}_{+0.2}$	$^{-1.1}_{+1.1}$	$^{+0.0}_{-0.0}$
3000	0.48	14	$3.01e-03$	$^{+30.3}_{-23.2}$	$^{+7.2}_{-6.9}$	$^{+6.4}_{-6.5}$	$^{-1.5}_{+2.6}$	$^{+0.0}_{+0.0}$	$^{-1.5}_{+1.5}$	$^{+0.1}_{-0.1}$
3500	0.12	100	$5.68e-02$	$^{+10.0}_{-10.0}$	$^{+3.4}_{-3.3}$	$^{+3.2}_{-3.1}$	$^{-0.8}_{+1.0}$	$^{-0.4}_{+0.4}$	$^{+0.3}_{-0.3}$	$^{+0.0}_{-0.0}$
3500	0.14	63	$3.40e-02$	$^{+12.6}_{-12.6}$	$^{+3.8}_{-3.6}$	$^{+3.4}_{-3.5}$	$^{-0.5}_{+1.2}$	$^{-0.3}_{+0.2}$	$^{+0.2}_{-0.2}$	$^{+0.0}_{-0.0}$
3500	0.18	78	$3.21e-02$	$^{+11.3}_{-11.3}$	$^{+4.1}_{-4.2}$	$^{+3.4}_{-3.5}$	$^{-1.6}_{+1.3}$	$^{-0.0}_{+0.1}$	$^{+1.6}_{-1.6}$	$^{+0.0}_{-0.0}$
3500	0.22	45	$1.82e-02$	$^{+14.9}_{-14.9}$	$^{+4.6}_{-4.0}$	$^{+4.7}_{-3.9}$	$^{-0.9}_{+1.2}$	$^{-0.3}_{+0.3}$	$^{+0.0}_{-0.0}$	$^{+0.0}_{-0.0}$
3500	0.26	42	$1.42e-02$	$^{+15.4}_{-15.4}$	$^{+4.4}_{-4.5}$	$^{+4.2}_{-4.3}$	$^{-0.1}_{+0.7}$	$^{-0.3}_{+0.3}$	$^{+0.2}_{-0.2}$	$^{+0.0}_{-0.0}$
3500	0.31	29	$1.00e-02$	$^{+18.6}_{-18.6}$	$^{+5.8}_{-5.5}$	$^{+5.1}_{-5.1}$	$^{-1.1}_{+1.7}$	$^{+0.1}_{+0.1}$	$^{-1.8}_{+1.8}$	$^{+0.0}_{-0.0}$
3500	0.37	26	$7.47e-03$	$^{+19.6}_{-19.6}$	$^{+6.2}_{-6.1}$	$^{+5.6}_{-5.6}$	$^{-1.8}_{+2.0}$	$^{-0.1}_{+0.3}$	$^{-1.4}_{+1.4}$	$^{+0.0}_{-0.0}$
3500	0.43	21	$5.83e-03$	$^{+21.8}_{-21.8}$	$^{+8.0}_{-7.5}$	$^{+6.9}_{-6.8}$	$^{-1.9}_{+2.4}$	$^{-0.1}_{+0.1}$	$^{-2.2}_{+2.2}$	$^{+0.1}_{-0.1}$
3500	0.52	24	$3.32e-03$	$^{+20.4}_{-20.4}$	$^{+7.1}_{-7.4}$	$^{+7.0}_{-7.0}$	$^{-1.8}_{+1.2}$	$^{-0.0}_{-0.1}$	$^{+0.2}_{-0.2}$	$^{+0.1}_{-0.1}$
4150	0.11	55	$3.51e-02$	$^{+13.5}_{-13.5}$	$^{+4.1}_{-4.5}$	$^{+3.8}_{-4.0}$	$^{-1.6}_{+0.5}$	$^{-0.2}_{+0.4}$	$^{-1.3}_{+1.3}$	$^{+0.0}_{-0.0}$
4150	0.14	54	$2.71e-02$	$^{+13.6}_{-13.6}$	$^{+4.4}_{-4.3}$	$^{+4.1}_{-4.1}$	$^{-1.6}_{+1.3}$	$^{-0.7}_{+0.5}$	$^{-0.0}_{+0.0}$	$^{+0.0}_{-0.0}$
4150	0.17	67	$2.39e-02$	$^{+12.2}_{-12.2}$	$^{+4.0}_{-4.6}$	$^{+3.7}_{-3.8}$	$^{-0.6}_{+0.6}$	$^{-0.0}_{+0.2}$	$^{+1.4}_{-1.4}$	$^{+0.0}_{-0.0}$
4150	0.21	53	$1.82e-02$	$^{+13.7}_{-13.7}$	$^{+4.5}_{-4.3}$	$^{+4.2}_{-4.2}$	$^{-0.0}_{+0.8}$	$^{+0.0}_{+0.2}$	$^{-0.3}_{+0.3}$	$^{+0.0}_{-0.0}$
4150	0.25	34	$9.75e-03$	$^{+17.1}_{-17.1}$	$^{+4.9}_{-4.9}$	$^{+4.5}_{-4.5}$	$^{-1.7}_{+1.3}$	$^{-0.6}_{+0.3}$	$^{-0.6}_{+0.6}$	$^{+0.0}_{-0.0}$
4150	0.31	21	$5.97e-03$	$^{+21.8}_{-21.8}$	$^{+5.5}_{-5.7}$	$^{+5.3}_{-5.3}$	$^{-1.7}_{+0.9}$	$^{+0.2}_{-0.1}$	$^{-0.5}_{+0.5}$	$^{+0.0}_{-0.0}$
4150	0.36	23	$5.95e-03$	$^{+20.9}_{-20.9}$	$^{+6.5}_{-7.2}$	$^{+6.1}_{-6.4}$	$^{-1.6}_{-0.8}$	$^{-0.3}_{+0.2}$	$^{+2.0}_{-2.0}$	$^{+0.0}_{-0.0}$
4150	0.42	16	$3.62e-03$	$^{+28.1}_{-21.9}$	$^{+8.5}_{-7.1}$	$^{+7.6}_{-7.1}$	$^{-0.4}_{+2.8}$	$^{-0.2}_{+0.4}$	$^{-0.2}_{+0.2}$	$^{+0.1}_{-0.1}$
4150	0.48	9	$2.23e-03$	$^{+39.0}_{-27.9}$	$^{+14.6}_{-10.6}$	$^{+17.8}_{-10.1}$	$^{-2.0}_{+1.4}$	$^{+0.0}_{-0.2}$	$^{-3.1}_{+3.1}$	$^{+0.1}_{-0.1}$
4150	0.57	12	$1.36e-03$	$^{+33.1}_{-24.7}$	$^{+10.8}_{-10.3}$	$^{+10.2}_{-9.8}$	$^{-2.8}_{+3.4}$	$^{+0.0}_{-0.1}$	$^{-1.7}_{+1.7}$	$^{+0.2}_{-0.2}$

Table 2: Continuation 3.

Q^2 (GeV^2)	x	N	$d^2\sigma/dxdQ^2$ ($\mathrm{pb/GeV}^2$)	δ_{stat} (%)	δ_{sys} (%)	δ_{u} (%)	δ_1 (%)	δ_2 (%)	δ_3 (%)	δ_4 (%)
5250	0.11	60	$1.87e-02$	$^{+12.9}_{-12.9}$	$^{+4.1}_{-4.8}$	$^{+3.7}_{-3.7}$	$^{-1.1}_{+1.1}$	$^{-0.3}_{-0.2}$	$^{+1.4}_{-1.4}$	$^{+0.0}_{-0.0}$
5250	0.14	74	$1.81e-02$	$^{+11.6}_{-11.6}$	$^{+4.7}_{-3.9}$	$^{+3.6}_{-3.6}$	$^{-1.3}_{+1.6}$	$^{-0.5}_{+1.0}$	$^{-0.5}_{+0.5}$	$^{+0.0}_{-0.0}$
5250	0.17	60	$1.35e-02$	$^{+12.9}_{-12.9}$	$^{+4.5}_{-4.0}$	$^{+3.9}_{-3.9}$	$^{-0.8}_{+1.4}$	$^{-0.2}_{+0.2}$	$^{-0.3}_{+0.3}$	$^{+0.0}_{-0.0}$
5250	0.20	50	$8.51e-03$	$^{+14.1}_{-14.1}$	$^{+4.2}_{-4.5}$	$^{+3.8}_{-3.8}$	$^{-1.7}_{+1.0}$	$^{-0.3}_{+0.3}$	$^{+1.0}_{-1.0}$	$^{+0.0}_{-0.0}$
5250	0.25	66	$8.84e-03$	$^{+12.3}_{-12.3}$	$^{+4.2}_{-4.1}$	$^{+3.9}_{-3.9}$	$^{-0.9}_{+1.4}$	$^{-0.3}_{+0.1}$	$^{-0.3}_{+0.3}$	$^{+0.0}_{-0.0}$
5250	0.29	36	$4.92e-03$	$^{+16.7}_{-16.7}$	$^{+5.0}_{-5.1}$	$^{+4.7}_{-4.6}$	$^{-1.3}_{+1.1}$	$^{-0.1}_{+0.1}$	$^{+1.2}_{-1.2}$	$^{+0.0}_{-0.0}$
5250	0.35	33	$3.77e-03$	$^{+17.4}_{-17.4}$	$^{+5.8}_{-5.6}$	$^{+5.1}_{-5.1}$	$^{-1.3}_{+1.7}$	$^{-0.3}_{+0.5}$	$^{-1.6}_{+1.6}$	$^{+0.0}_{-0.0}$
5250	0.41	13	$1.55e-03$	$^{+31.5}_{-23.9}$	$^{+7.7}_{-7.3}$	$^{+6.5}_{-6.5}$	$^{-2.8}_{+3.6}$	$^{-0.2}_{+0.4}$	$^{-0.0}_{+0.0}$	$^{+0.0}_{-0.0}$
5250	0.47	13	$1.52e-03$	$^{+31.5}_{-23.9}$	$^{+8.9}_{-8.9}$	$^{+8.1}_{-8.1}$	$^{-1.8}_{+2.2}$	$^{-0.7}_{+0.1}$	$^{-3.1}_{+3.1}$	$^{+0.1}_{-0.1}$
5250	0.53	12	$1.22e-03$	$^{+33.1}_{-24.8}$	$^{+13.2}_{-11.5}$	$^{+10.0}_{-9.6}$	$^{-0.0}_{+3.7}$	$^{+0.1}_{+0.3}$	$^{-6.3}_{+6.3}$	$^{+0.1}_{-0.1}$
5250	0.62	13	$5.79e-04$	$^{+31.5}_{-23.9}$	$^{+11.5}_{-13.0}$	$^{+10.5}_{-10.5}$	$^{-5.9}_{+4.3}$	$^{+0.1}_{-0.1}$	$^{+0.9}_{-0.9}$	$^{+0.6}_{-0.6}$
7000	0.12	45	$1.05e-02$	$^{+14.9}_{-14.9}$	$^{+5.8}_{-5.4}$	$^{+4.9}_{-4.9}$	$^{-0.3}_{+1.4}$	$^{+0.4}_{+0.1}$	$^{+1.1}_{-1.1}$	$^{+0.0}_{-0.0}$
7000	0.14	34	$6.44e-03$	$^{+17.2}_{-17.2}$	$^{+5.1}_{-6.1}$	$^{+4.7}_{-5.0}$	$^{-2.1}_{+1.4}$	$^{-0.4}_{+0.1}$	$^{-0.5}_{+0.5}$	$^{+0.0}_{-0.0}$
7000	0.18	40	$5.72e-03$	$^{+15.8}_{-15.8}$	$^{+4.9}_{-5.4}$	$^{+4.6}_{-4.7}$	$^{-1.8}_{+0.8}$	$^{-0.3}_{+0.2}$	$^{-1.3}_{+1.3}$	$^{+0.0}_{-0.0}$
7000	0.22	37	$4.76e-03$	$^{+16.4}_{-16.4}$	$^{+6.0}_{-6.6}$	$^{+4.9}_{-5.0}$	$^{-1.1}_{+1.6}$	$^{-0.4}_{+0.3}$	$^{-2.9}_{+2.9}$	$^{+0.0}_{-0.0}$
7000	0.26	28	$2.95e-03$	$^{+18.9}_{-18.9}$	$^{+5.5}_{-6.0}$	$^{+5.1}_{-5.2}$	$^{-1.7}_{+1.3}$	$^{-0.6}_{+0.4}$	$^{-0.6}_{+0.6}$	$^{+0.0}_{-0.0}$
7000	0.32	27	$2.33e-03$	$^{+19.2}_{-19.2}$	$^{+6.7}_{-5.7}$	$^{+5.6}_{-5.5}$	$^{-0.6}_{+2.5}$	$^{+0.2}_{+0.4}$	$^{-1.3}_{+1.3}$	$^{+0.0}_{-0.0}$
7000	0.38	13	$1.20e-03$	$^{+31.5}_{-23.9}$	$^{+7.2}_{-8.0}$	$^{+7.2}_{-7.4}$	$^{-2.6}_{-0.1}$	$^{-0.6}_{+0.3}$	$^{-1.2}_{+1.2}$	$^{+0.0}_{-0.0}$
7000	0.44	5	$4.45e-04$	$^{+55.2}_{-35.2}$	$^{+9.2}_{-8.9}$	$^{+8.5}_{-8.6}$	$^{-2.1}_{+2.1}$	$^{-0.3}_{+0.3}$	$^{+1.1}_{-1.1}$	$^{+0.1}_{-0.1}$
7000	0.50	10	$8.55e-04$	$^{+36.7}_{-26.8}$	$^{+13.5}_{-11.9}$	$^{+11.7}_{-10.6}$	$^{-2.6}_{+5.1}$	$^{-0.5}_{+0.4}$	$^{-4.4}_{+4.4}$	$^{+0.1}_{-0.1}$
7000	0.56	6	$5.30e-04$	$^{+49.5}_{-32.8}$	$^{+14.8}_{-15.7}$	$^{+14.2}_{-14.7}$	$^{-2.2}_{+0.1}$	$^{+0.7}_{-0.0}$	$^{+4.1}_{-4.1}$	$^{+0.2}_{-0.2}$
7000	0.66	1	$2.74e-05$	$^{+158.0}_{-58.0}$	$^{+16.6}_{-14.5}$	$^{+14.0}_{-13.8}$	$^{-1.4}_{+5.6}$	$^{+0.1}_{+0.0}$	$^{+4.1}_{-4.1}$	$^{+0.9}_{-0.9}$
9500	0.17	19	$2.20e-03$	$^{+25.5}_{-20.3}$	$^{+9.3}_{-11.0}$	$^{+6.3}_{-6.3}$	$^{-2.2}_{+1.4}$	$^{+0.1}_{-0.4}$	$^{+0.2}_{-0.2}$	$^{+0.0}_{-0.0}$
9500	0.21	24	$2.30e-03$	$^{+20.4}_{-20.4}$	$^{+7.6}_{-6.4}$	$^{+6.2}_{-6.2}$	$^{-0.5}_{+2.2}$	$^{-0.8}_{+0.6}$	$^{-0.5}_{+0.5}$	$^{+0.0}_{-0.0}$
9500	0.25	23	$1.78e-03$	$^{+20.9}_{-20.9}$	$^{+6.9}_{-6.4}$	$^{+6.3}_{-6.3}$	$^{-0.7}_{+1.4}$	$^{-0.5}_{+0.5}$	$^{-0.0}_{+0.0}$	$^{+0.0}_{-0.0}$
9500	0.31	15	$1.11e-03$	$^{+29.1}_{-22.5}$	$^{+10.1}_{-8.0}$	$^{+10.9}_{-7.0}$	$^{-1.9}_{+1.0}$	$^{-0.6}_{+0.2}$	$^{-3.1}_{+3.1}$	$^{+0.0}_{-0.0}$
9500	0.36	14	$8.82e-04$	$^{+30.3}_{-23.2}$	$^{+11.1}_{-8.0}$	$^{+7.8}_{-7.8}$	$^{-0.7}_{+2.2}$	$^{+0.6}_{+0.8}$	$^{-1.6}_{+1.6}$	$^{+0.0}_{-0.0}$
9500	0.42	9	$5.67e-04$	$^{+39.0}_{-27.9}$	$^{+9.8}_{-10.2}$	$^{+9.5}_{-9.5}$	$^{-3.1}_{+1.4}$	$^{-1.2}_{+0.1}$	$^{+0.3}_{-0.3}$	$^{+0.0}_{-0.0}$
9500	0.48	8	$5.09e-04$	$^{+41.8}_{-29.4}$	$^{+12.5}_{-12.4}$	$^{+12.2}_{-12.0}$	$^{-1.8}_{+2.1}$	$^{-0.6}_{+0.2}$	$^{+1.2}_{-1.2}$	$^{+0.1}_{-0.1}$
9500	0.54	7	$3.99e-04$	$^{+45.1}_{-31.0}$	$^{+15.1}_{-15.3}$	$^{+14.6}_{-14.9}$	$^{-2.0}_{+1.8}$	$^{-0.8}_{+0.8}$	$^{-3.2}_{+3.2}$	$^{+0.1}_{-0.1}$
9500	0.61	2	$1.03e-04$	$^{+98.5}_{-48.5}$	$^{+19.8}_{-21.0}$	$^{+19.3}_{-19.6}$	$^{-6.0}_{+1.3}$	$^{-0.4}_{+0.2}$	$^{+4.3}_{-4.3}$	$^{+0.4}_{-0.4}$
9500	0.71	0	$< 3.37e-05$							

Table 2: Continuation 4.

Q^2 (GeV^2)	x	N	$d^2\sigma/dxdQ^2$ ($\mathrm{pb/GeV}^2$)	δ_{stat} (%)	δ_{sys} (%)	δ_{u} (%)	δ_1 (%)	δ_2 (%)	δ_3 (%)	δ_4 (%)
15500	0.43	41	$1.57e-04$	$^{+15.6}_{-15.6}$	$^{+6.6}_{-5.4}$	$^{+4.8}_{-4.5}$	$^{-2.6}_{+2.7}$	$^{-0.6}_{+0.6}$	$^{-0.3}_{+0.3}$	$^{+0.1}_{-0.1}$
15500	0.80	3	$1.72e-06$	$^{+75.7}_{-42.3}$	$^{+18.5}_{-17.7}$	$^{+16.7}_{-16.7}$	$^{-4.8}_{+5.1}$	$^{-0.6}_{+0.2}$	$^{-0.6}_{+0.6}$	$^{+2.4}_{-2.4}$

Table 2: Continuation 5.

Q^2 (GeV^2)	$x_{\rm edge}$	N	$I(x)$ (pb/GeV^2)	$\delta_{\rm stat}$ (%)	$\delta_{\rm sys}$ (%)	$\delta_{\rm u}$ (%)	δ_1 (%)	δ_2 (%)	δ_3 (%)	δ_4 (%)
725	0.63	504	$7.71e-02$	$^{+4.5}_{-4.5}$	$^{+2.8}_{-3.2}$	$^{+1.5}_{-1.3}$	$^{+1.3}_{-2.0}$	$^{+0.0}_{-0.1}$	$^{+1.9}_{-1.9}$	$^{+0.3}_{-0.3}$
875	0.64	671	$5.12e-02$	$^{+3.9}_{-3.9}$	$^{+2.3}_{-1.9}$	$^{+1.2}_{-1.2}$	$^{-0.1}_{+1.0}$	$^{+0.0}_{-0.0}$	$^{+1.3}_{-1.3}$	$^{+0.5}_{-0.5}$
1025	0.66	414	$2.75e-02$	$^{+4.9}_{-4.9}$	$^{+3.4}_{-3.6}$	$^{+1.5}_{-1.5}$	$^{-1.6}_{+0.8}$	$^{+0.0}_{-0.0}$	$^{+2.7}_{-2.7}$	$^{+0.6}_{-0.6}$
1200	0.67	368	$1.80e-02$	$^{+5.2}_{-5.2}$	$^{+3.7}_{-2.9}$	$^{+1.7}_{-1.6}$	$^{-1.5}_{+2.5}$	$^{+0.0}_{-0.0}$	$^{+1.4}_{-1.4}$	$^{+0.8}_{-0.8}$
1400	0.68	202	$1.04e-02$	$^{+7.0}_{-7.0}$	$^{+3.5}_{-3.8}$	$^{+2.1}_{-2.0}$	$^{-1.8}_{+1.3}$	$^{+0.0}_{-0.0}$	$^{+2.1}_{-2.1}$	$^{+1.0}_{-1.0}$
1650	0.69	173	$5.91e-03$	$^{+7.6}_{-7.6}$	$^{+4.4}_{-4.1}$	$^{+2.3}_{-2.2}$	$^{-1.7}_{+2.0}$	$^{+0.1}_{-0.1}$	$^{+2.6}_{-2.6}$	$^{+1.2}_{-1.2}$
1950	0.71	74	$2.51e-03$	$^{+11.6}_{-11.6}$	$^{+5.2}_{-5.1}$	$^{+3.1}_{-3.0}$	$^{-1.9}_{+1.9}$	$^{+0.0}_{-0.1}$	$^{+3.1}_{-3.1}$	$^{+1.6}_{-1.6}$
2250	0.73	51	$1.84e-03$	$^{+14.0}_{-14.0}$	$^{+7.1}_{-7.6}$	$^{+4.1}_{-4.1}$	$^{-3.0}_{+2.2}$	$^{+0.0}_{-0.0}$	$^{+4.9}_{-4.9}$	$^{+2.0}_{-2.0}$
2600	0.75	36	$9.65e-04$	$^{+16.7}_{-16.7}$	$^{+6.9}_{-6.6}$	$^{+4.8}_{-4.8}$	$^{-1.9}_{+2.6}$	$^{+0.0}_{-0.0}$	$^{+3.0}_{-3.0}$	$^{+2.5}_{-2.5}$
3000	0.77	19	$4.90e-04$	$^{+25.5}_{-20.3}$	$^{+11.0}_{-10.9}$	$^{+6.6}_{-6.6}$	$^{-3.9}_{+4.1}$	$^{+0.1}_{-0.1}$	$^{+6.8}_{-6.8}$	$^{+3.2}_{-3.2}$
3500	0.79	17	$3.01e-04$	$^{+27.2}_{-21.3}$	$^{+11.6}_{-11.5}$	$^{+8.0}_{-7.8}$	$^{-3.3}_{+3.5}$	$^{+0.1}_{-0.2}$	$^{+6.4}_{-6.4}$	$^{+4.0}_{-4.0}$
4150	0.81	5	$8.19e-05$	$^{+55.2}_{-35.2}$	$^{+14.6}_{-15.0}$	$^{+11.9}_{-11.8}$	$^{-3.7}_{+2.1}$	$^{+0.0}_{-0.3}$	$^{+6.4}_{-6.4}$	$^{+5.1}_{-5.1}$
5250	0.85	3	$1.98e-05$	$^{+75.7}_{-42.3}$	$^{+18.6}_{-18.1}$	$^{+14.3}_{-14.3}$	$^{-2.9}_{+4.7}$	$^{+0.2}_{+0.0}$	$^{+8.1}_{-8.1}$	$^{+6.9}_{-6.9}$
7000	0.87	1	$5.56e-06$	$^{+158.0}_{-58.0}$	$^{+29.0}_{-26.4}$	$^{+24.3}_{-24.1}$	$^{-3.7}_{+10.7}$	$^{-0.4}_{+0.0}$	$^{-1.3}_{+1.3}$	$^{+9.4}_{-9.4}$
9500	0.89	1	$5.60e-06$	$^{+158.0}_{-58.0}$	$^{+58.3}_{-63.4}$	$^{+53.5}_{-53.5}$	$^{-19.0}_{-0.7}$	$^{+0.0}_{+0.0}$	$^{+19.2}_{-19.2}$	$^{+13.0}_{-13.0}$

Table 3: The integrated cross section, $I(x)$ (see Eq.(11)), for NC e^-p scattering at $\sqrt{s} = 318\,\text{GeV}$ as a function of Q^2. Also quoted are the lower limit of integration, $x_{\rm edge}$, the number of events reconstructed in the bin, N, the statistical uncertainty, $\delta_{\rm stat}$, the total systematic uncertainty, $\delta_{\rm sys}$, the total uncorrelated systematic uncertainty, $\delta_{\rm u}$, followed by the bin-to-bin correlated systematic uncertainties, δ_1–δ_4 defined in Section 9. The luminosity uncertainty of 1.8% is not included.

Q^2 (GeV^2)	$x_{\rm edge}$	N	$I(x)$ (pb/GeV^2)	$\delta_{\rm stat}$ (%)	$\delta_{\rm sys}$ (%)	$\delta_{\rm u}$ (%)	δ_1 (%)	δ_2 (%)	δ_3 (%)	δ_4 (%)
725	0.63	371	$7.50e-02$	$^{+5.2}_{-5.2}$	$^{+2.4}_{-2.3}$	$^{+1.7}_{-1.4}$	$^{+1.2}_{-1.3}$	$^{+0.1}_{-0.1}$	$^{+0.8}_{-0.8}$	$^{+0.3}_{-0.3}$
875	0.64	482	$4.81e-02$	$^{+4.6}_{-4.6}$	$^{+1.9}_{-1.7}$	$^{+1.6}_{-1.3}$	$^{-0.5}_{+0.6}$	$^{+0.1}_{-0.1}$	$^{-0.1}_{+0.1}$	$^{+0.4}_{-0.4}$
1025	0.66	281	$2.50e-02$	$^{+6.0}_{-6.0}$	$^{+3.0}_{-2.4}$	$^{+1.7}_{-1.6}$	$^{-1.3}_{+1.8}$	$^{+0.0}_{-0.0}$	$^{+0.3}_{-0.3}$	$^{+0.5}_{-0.5}$
1200	0.67	275	$1.80e-02$	$^{+6.0}_{-6.0}$	$^{+3.1}_{-2.9}$	$^{+2.0}_{-1.8}$	$^{-1.5}_{+1.8}$	$^{+0.0}_{-0.0}$	$^{+0.9}_{-0.9}$	$^{+0.7}_{-0.7}$
1400	0.68	146	$9.99e-03$	$^{+8.3}_{-8.3}$	$^{+3.5}_{-3.7}$	$^{+2.4}_{-2.3}$	$^{-1.8}_{+1.7}$	$^{+0.0}_{-0.0}$	$^{+1.5}_{-1.5}$	$^{+0.8}_{-0.8}$
1650	0.69	115	$5.24e-03$	$^{+9.3}_{-9.3}$	$^{+3.5}_{-3.5}$	$^{+2.5}_{-2.5}$	$^{-1.9}_{+1.7}$	$^{+0.0}_{-0.1}$	$^{+0.7}_{-0.7}$	$^{+1.1}_{-1.1}$
1950	0.71	62	$2.86e-03$	$^{+12.7}_{-12.7}$	$^{+5.6}_{-5.0}$	$^{+3.8}_{-3.4}$	$^{-2.2}_{+3.0}$	$^{+0.1}_{-0.0}$	$^{+2.3}_{-2.3}$	$^{+1.4}_{-1.4}$
2250	0.73	31	$1.47e-03$	$^{+18.0}_{-18.0}$	$^{+5.6}_{-5.9}$	$^{+4.6}_{-4.5}$	$^{-2.5}_{+2.1}$	$^{+0.0}_{-0.1}$	$^{+1.6}_{-1.6}$	$^{+1.7}_{-1.7}$
2600	0.75	27	$9.47e-04$	$^{+19.2}_{-19.2}$	$^{+6.7}_{-6.7}$	$^{+5.4}_{-5.3}$	$^{-2.2}_{+2.3}$	$^{+0.0}_{-0.1}$	$^{+2.6}_{-2.6}$	$^{+1.9}_{-1.9}$
3000	0.77	13	$4.63e-04$	$^{+31.5}_{-23.9}$	$^{+10.4}_{-10.7}$	$^{+7.6}_{-7.5}$	$^{-3.1}_{+2.4}$	$^{+0.0}_{+0.0}$	$^{+6.3}_{-6.3}$	$^{+2.1}_{-2.1}$
3500	0.79	11	$2.61e-04$	$^{+34.7}_{-25.7}$	$^{+10.9}_{-10.6}$	$^{+8.7}_{-8.7}$	$^{-4.0}_{+4.7}$	$^{+0.1}_{-0.3}$	$^{+3.5}_{-3.5}$	$^{+2.4}_{-2.4}$
4150	0.81	6	$1.29e-04$	$^{+49.5}_{-32.8}$	$^{+13.5}_{-14.8}$	$^{+13.2}_{-13.1}$	$^{-3.2}_{+0.7}$	$^{+0.0}_{+0.0}$	$^{+0.0}_{-0.0}$	$^{+2.8}_{-2.8}$
5250	0.85	3	$2.99e-05$	$^{+75.7}_{-42.3}$	$^{+20.4}_{-19.6}$	$^{+17.1}_{-16.7}$	$^{-3.5}_{+5.7}$	$^{-0.2}_{+0.0}$	$^{+8.5}_{-8.5}$	$^{+3.7}_{-3.7}$
7000	0.87	0	$< 9.68e-06$							
9500	0.89	0	$< 2.10e-06$							

Table 4: The integrated cross section, $I(x)$ (see Eq.(11)), for NC e^+p scattering at $\sqrt{s} = 318\,\text{GeV}$ as a function of Q^2. Also quoted are the lower limit of integration, $x_{\rm edge}$, the number of events reconstructed in the bin, N, the statistical uncertainty, $\delta_{\rm stat}$, the total systematic uncertainty, $\delta_{\rm sys}$, the total uncorrelated systematic uncertainty, $\delta_{\rm u}$, followed by the bin-to-bin correlated systematic uncertainties, δ_1–δ_4 defined in Section 9. If no event is observed, the 68% upper limit is given. The luminosity uncertainty of 1.8% is not included.

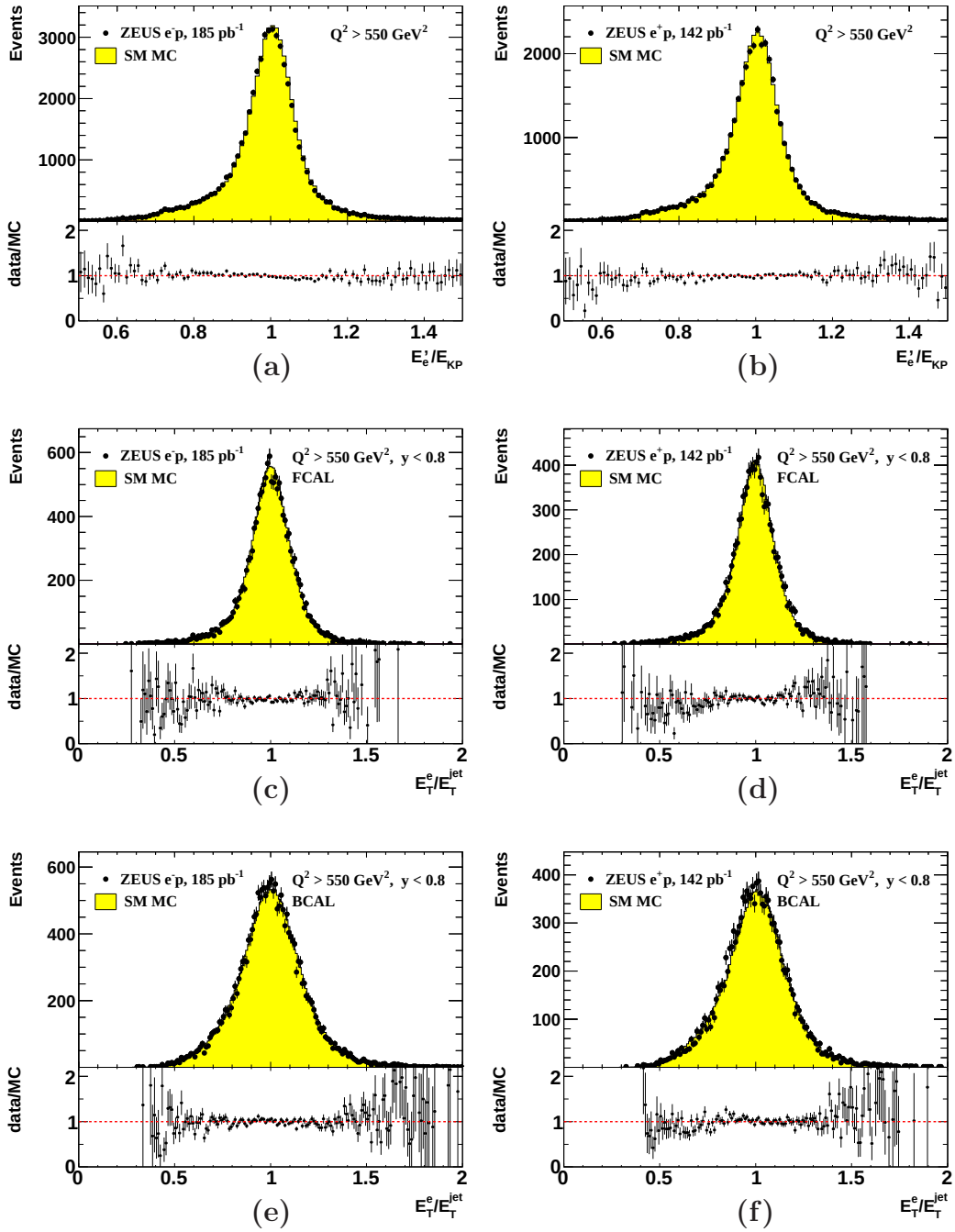

Figure 1: For e^-p and e^+p event samples with $Q^2 > 550\,\mathrm{GeV}^2$, distributions of (a), (b) the ratio of the measured electron energy, E'_e, to the expected energy, E_{KP}, for $y < 0.1$, (c), (d) of the transverse energy of the electron, E^e_T, to the transverse energy of the jet, E^{jet}_T, in one-jet events with $y < 0.8$ for jets in the FCAL and (e), (f) similarly for jets in the BCAL. In all upper panels, data samples are represented by dots while MC samples, normalised to the number of data events, are represented by histograms. The lower panels show the ratio of data to MC distributions.

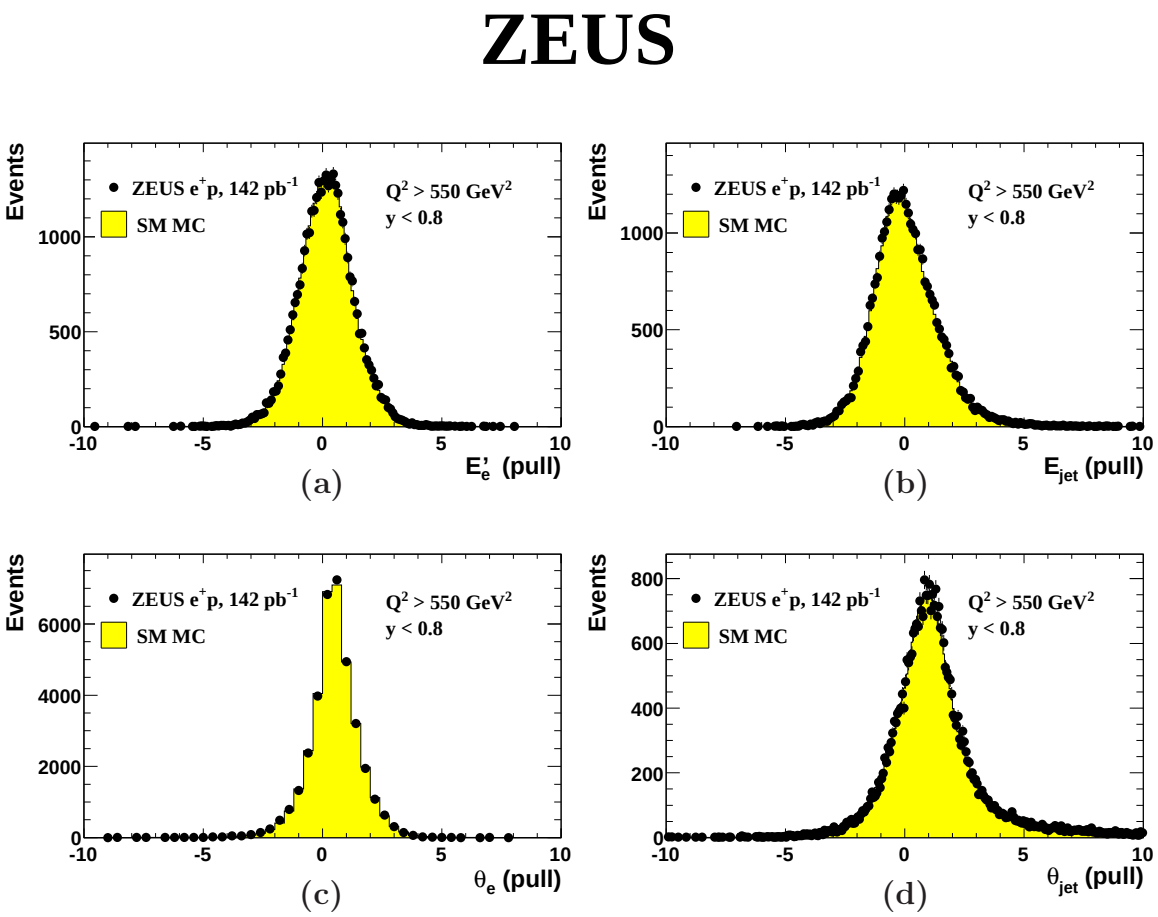

Figure 2: Distribution of the pulls obtained from the kinematic fit for (a) the electron energy, $E_e^{'}$, (b) jet energy, $E_{\rm jet}$, (c) electron scattering angle, θ_e, and (d) jet angle, $\theta_{\rm jet}$, in data (dots) compared to the corresponding distribution in MC (histogram) for the e^+p events with measured $Q^2 > 550\,{\rm GeV}^2$ and $y < 0.8$. The MC distributions are normalised to the number of events in the data.

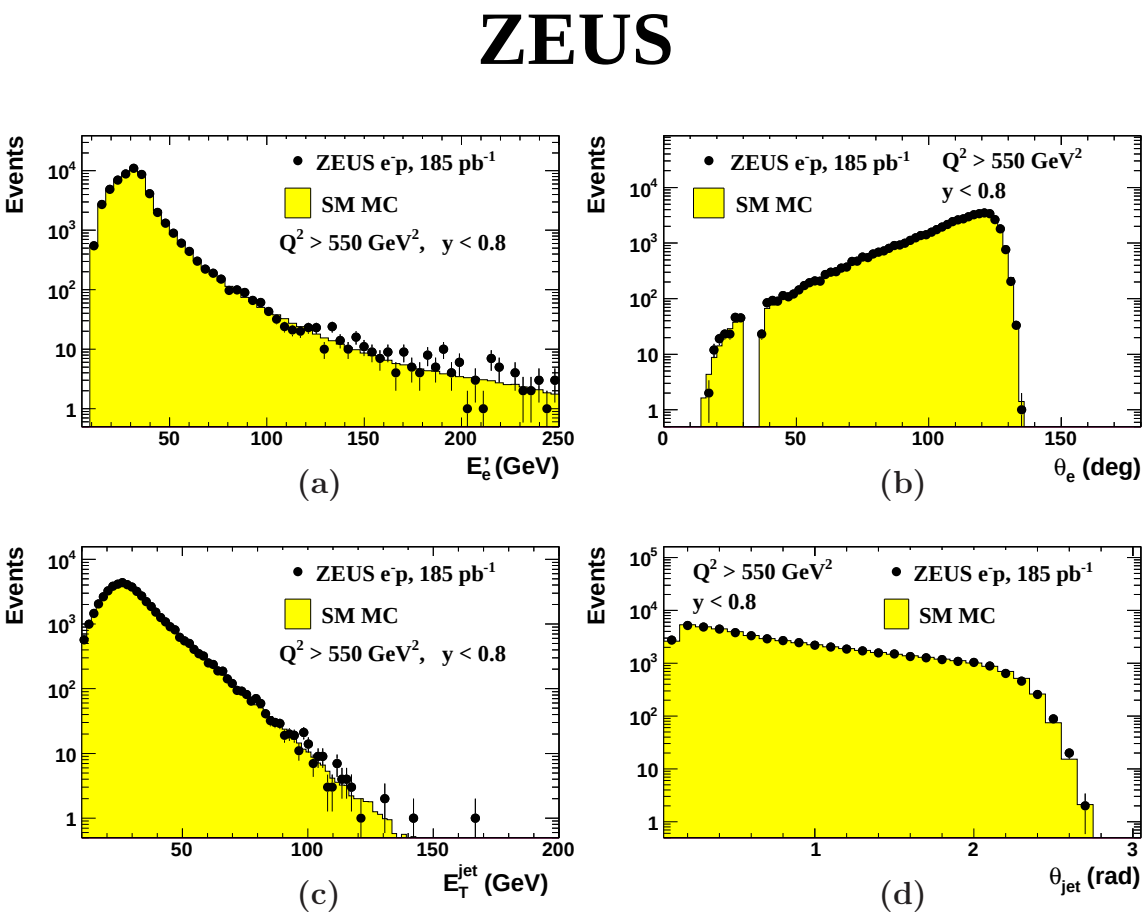

Figure 3: Distributions of (a) electron energy, E_e', (b) electron scattering angle, θ_e, (c) transverse energy of all jets, $E_T^{\rm jet}$, and (d) jet production angle, $\theta_{\rm jet}$, for e^-p events with $Q^2 > 550\,{\rm GeV}^2$ and $y < 0.8$ in data (dots) compared to the corresponding distributions in MC (histograms). The MC distributions are normalised to the number of events in the data.

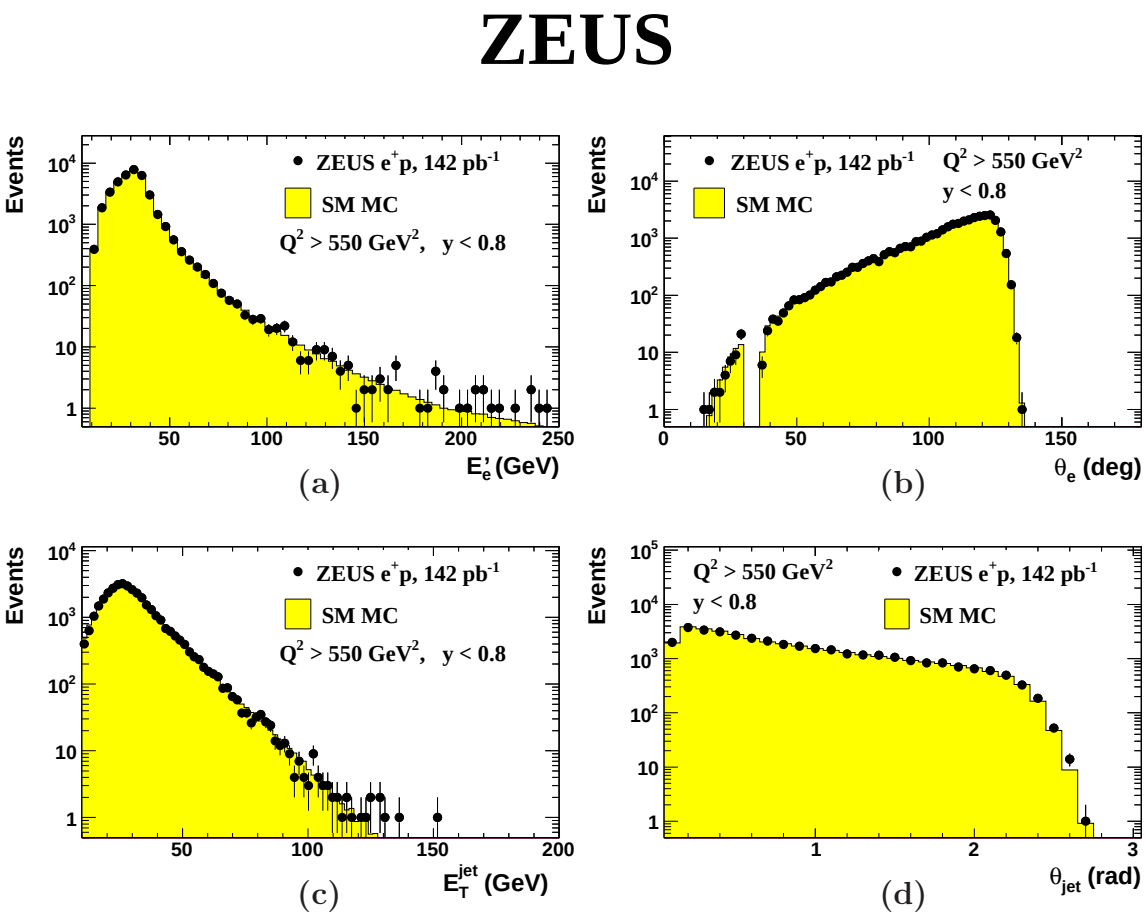

Figure 4: Distributions of (a) electron energy, $E_e^{'}$, (b) electron scattering angle, θ_e, (c) transverse energy of all jets, $E_T^{\rm jet}$, and (d) jet production angle, $\theta_{\rm jet}$, for e^+p events with $Q^2 > 550\,{\rm GeV}^2$ and $y < 0.8$ in data (dots) compared to the corresponding distributions in MC (histograms). The MC distributions are normalised to the number of events in the data.

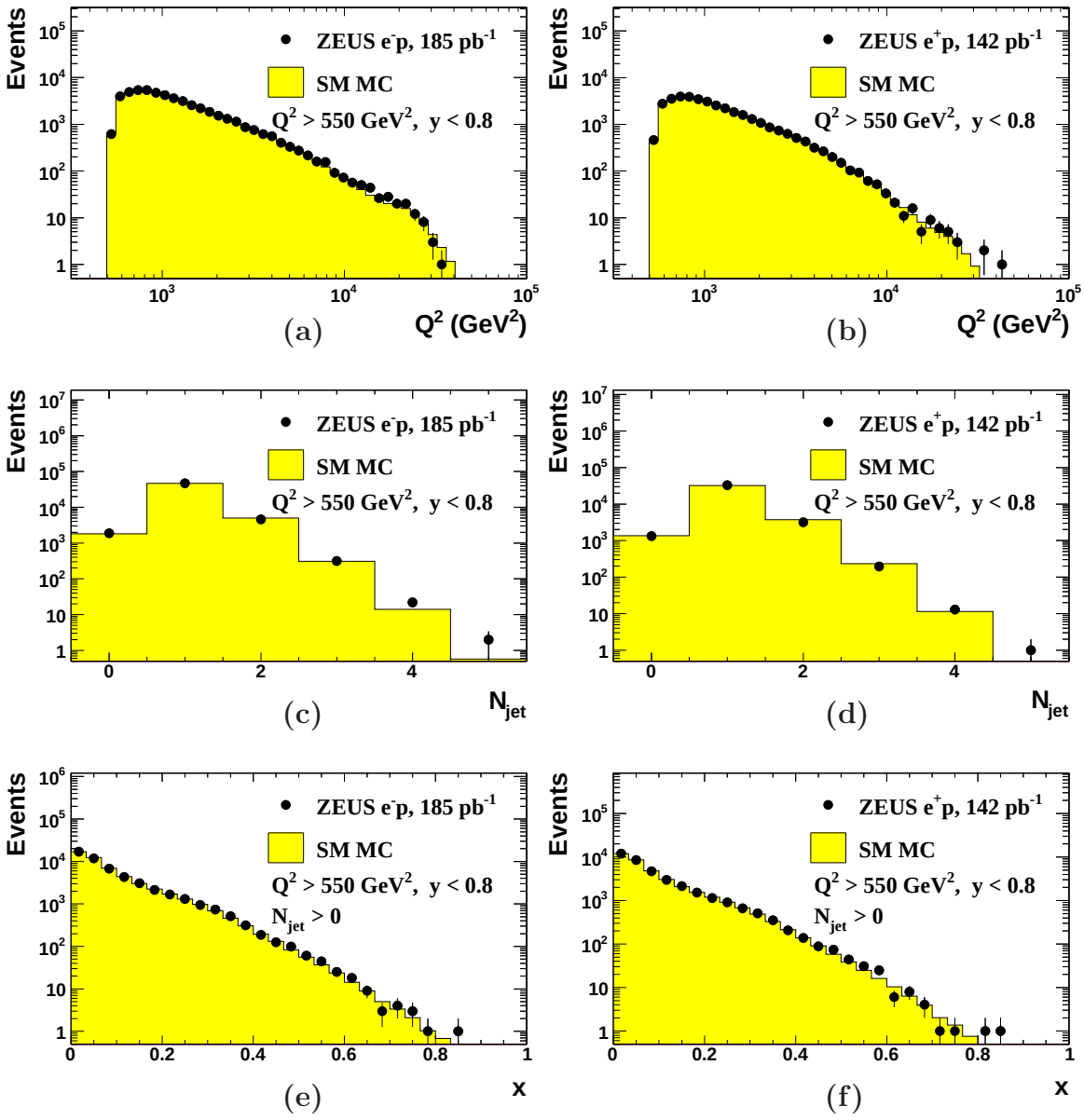

Figure 5: Distribution of (a), (b) Q^2, (c), (d) the jet multiplicity, $N_{\rm jet}$ and (e), (f) x for events with at least one jet for the e^-p and e^+p data samples (dots) for $Q^2 > 550\,\mathrm{GeV}^2$ and $y < 0.8$. The distributions are compared to MC expectations (histograms) normalised to the number of events in the data.

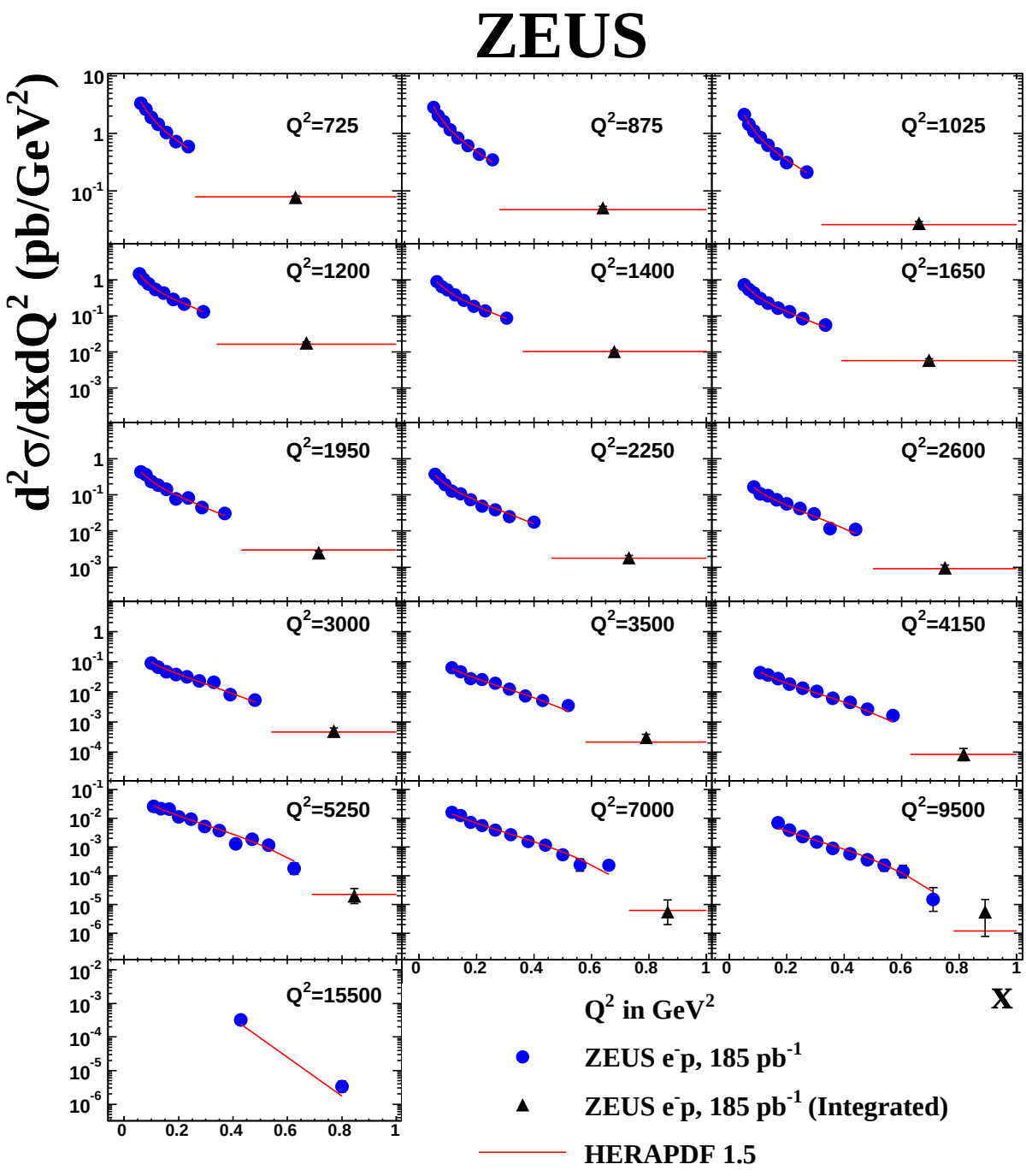

Figure 6: The double-differential cross section for NC e^-p scattering at $\sqrt{s} = 318\,\text{GeV}$ (dots) as a function of x and the double-differential cross section integrated over x divided by the bin width and placed at the centre of the bin (triangles) for different values of Q^2 as shown, compared to the Standard Model expectations evaluated using HERAPDF1.5 PDFs (line). The error bars show the statistical and systematic uncertainties added in quadrature.

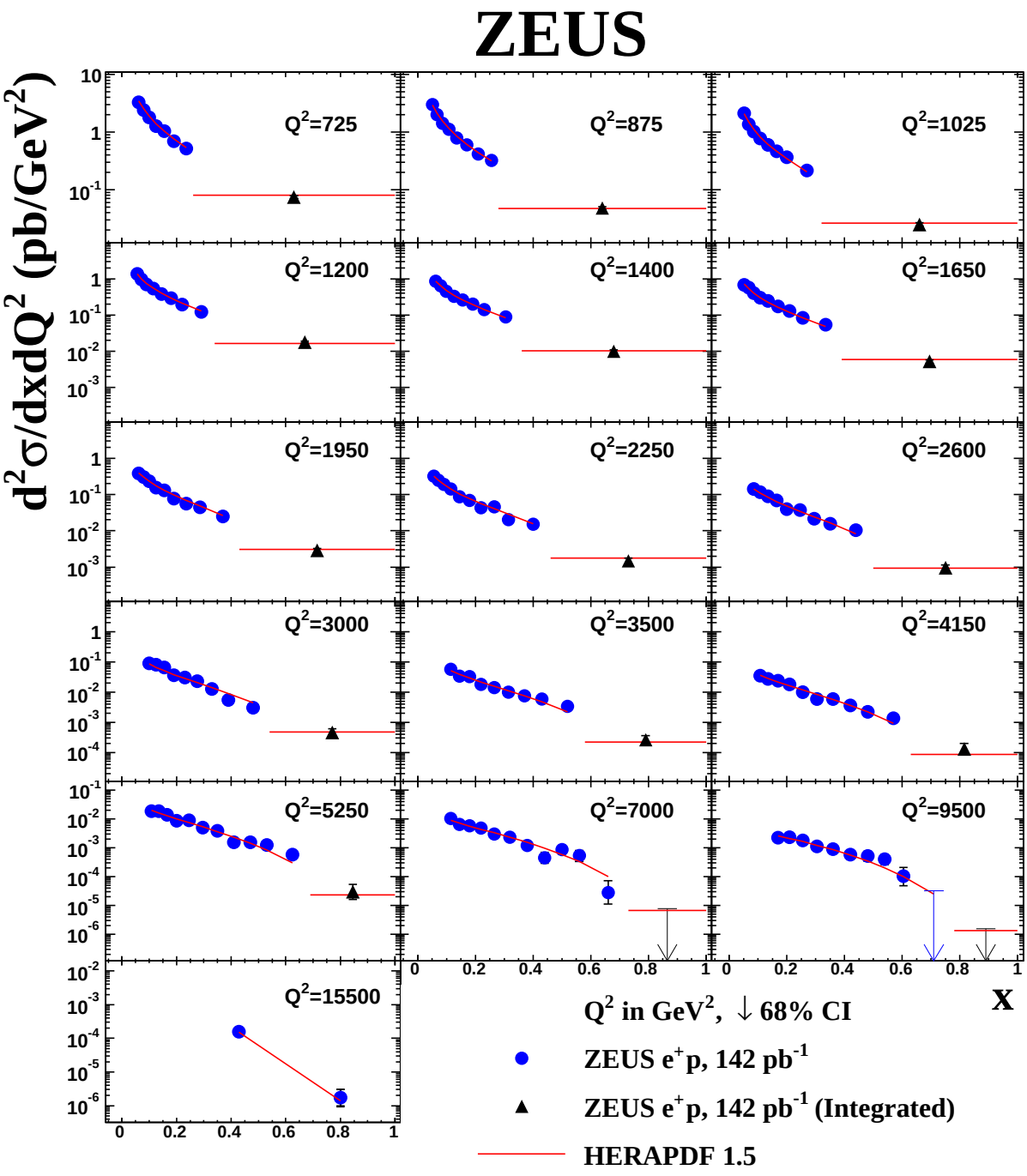

Figure 7: The double-differential cross section for NC e^+p scattering at $\sqrt{s} = 318\,\text{GeV}$ (dots) as a function of x and the double-differential cross section integrated over x divided by the bin width and placed at the centre of the bin (triangles) for different values of Q^2 as shown, compared to the Standard Model expectations evaluated using HERAPDF1.5 PDFs (line). The error bars show the statistical and systematic uncertainties added in quadrature. For bins with zero measured events, a 68% probability limit is given.

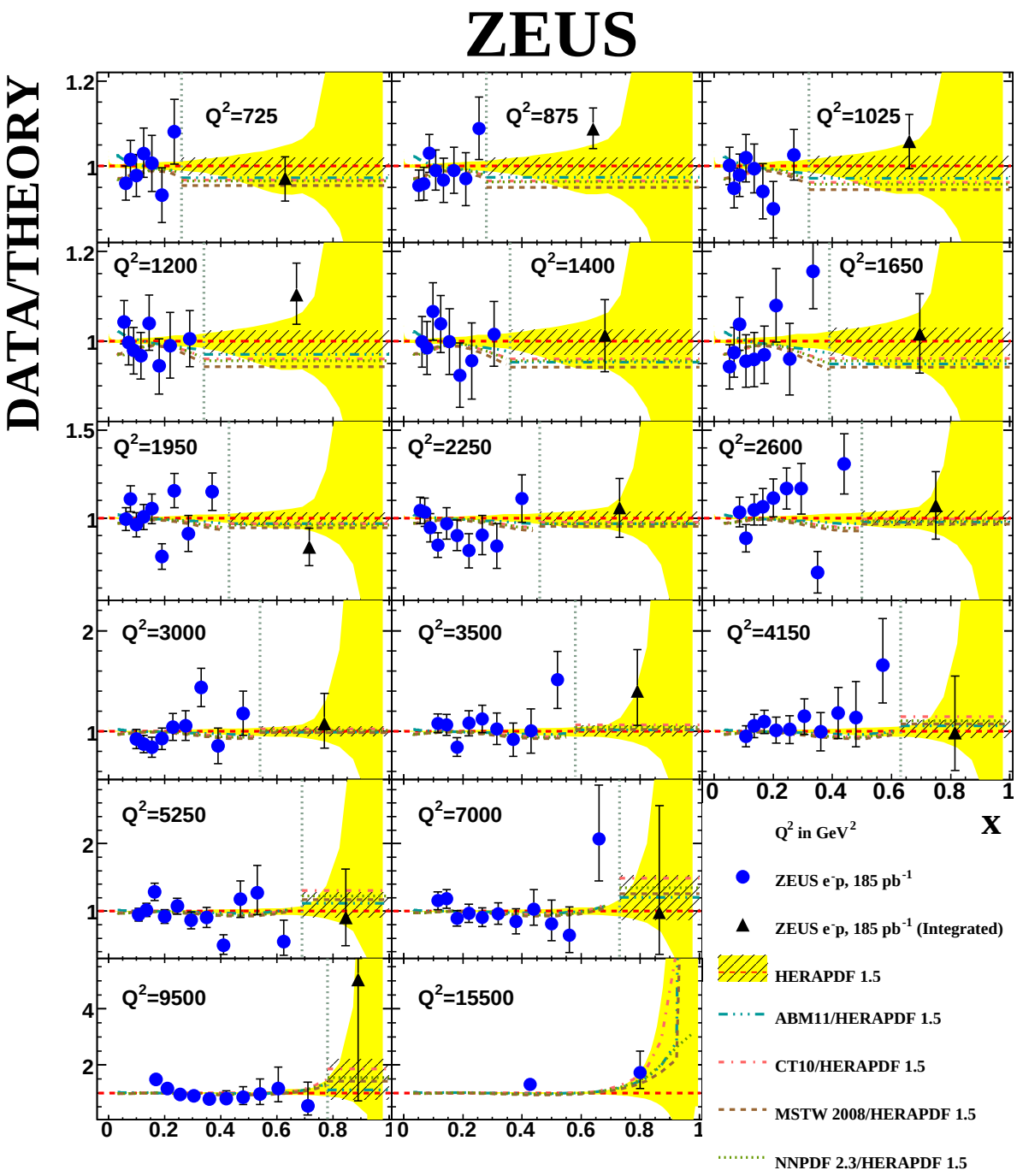

Figure 8: Ratio of the double-differential cross section for NC e^-p scattering and of the double-differential cross section integrated over x to the Standard Model expectation evaluated using the HERAPDF1.5 PDFs as a function of x at different Q^2 values as described in the legend. For HERAPDF1.5, the uncertainty is given as a band. The expectation for the integrated bin is also shown as a hatched box. The error bars show the statistical and systematic uncertainties added in quadrature. The expectations of other commonly used PDF sets normalised to HERAPDF1.5 PDFs are also shown, as listed in the legend. Note that the scale on the y axis changes with Q^2.

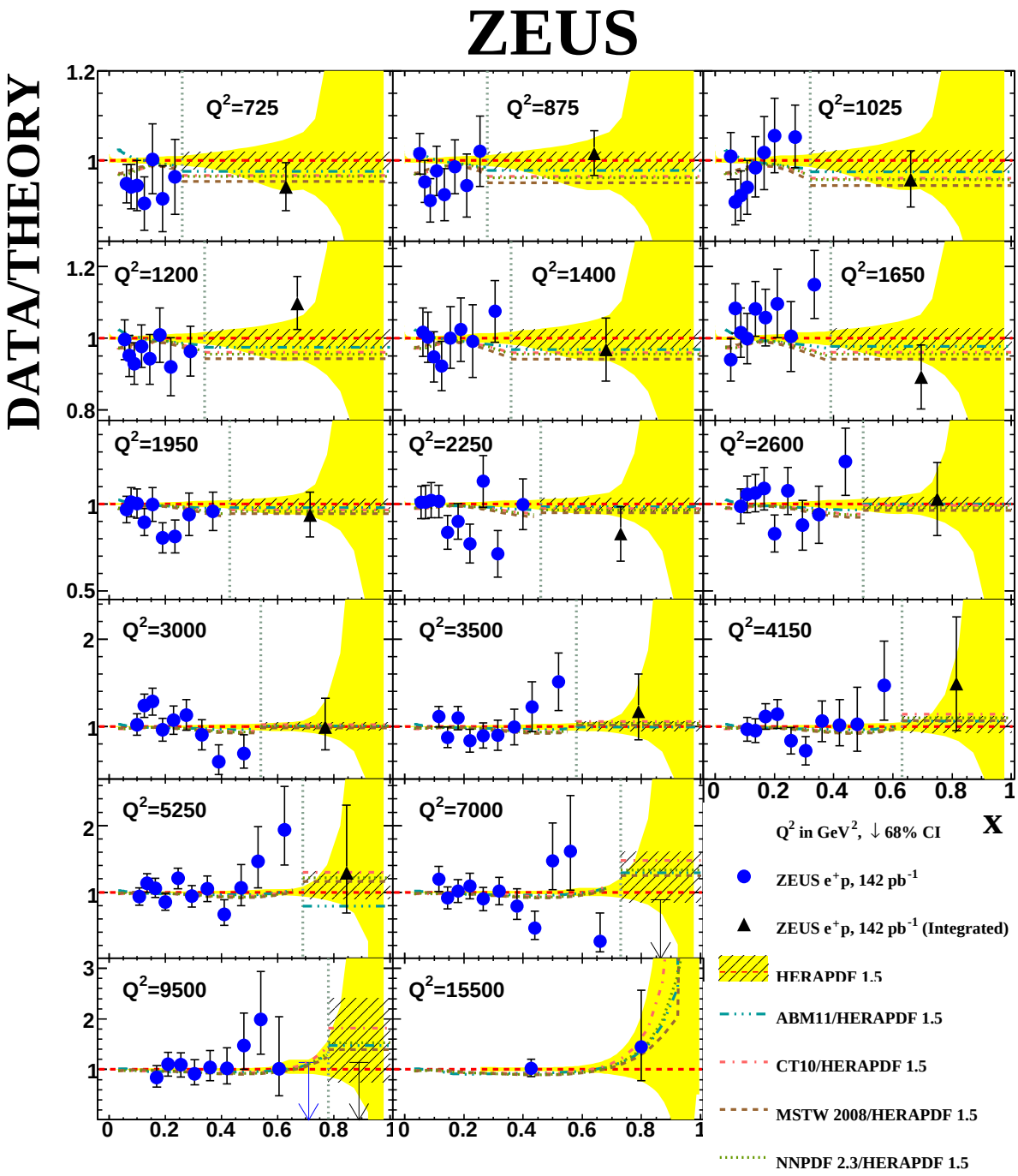

Figure 9: Ratio of the double-differential cross section for NC e^+p scattering and of the double-differential cross section integrated over x to the Standard Model expectation evaluated using the HERPDF1.5 PDFs as a function of x at different Q^2 values as described in the legend.For HERAPDF1.5, the uncertainty is given as a band. The expectation for the integrated bin is also shown as a hatched box. The error bars show the statistical and systematic uncertainties added in quadrature. For bins with zero measured events, a 68% probability limit is given. The expectations of other commonly used PDF sets normalised to HERAPDF1.5 PDFs are also shown, as listed in the legend. Note that the scale on the y axis changes with Q^2.